New insights on the early Mesozoic evolution of multiple tectonic regimes in the northeastern North China Craton from the detrital zircon provenance of sedimentary strata

Yi Ni Wang[1], Wen Liang Xu[1,2], Feng Wang[1], Xiao Bo Li[1]

[1] College of Earth Sciences, Jilin University, Changchun, 130061, China

[2] Key Laboratory of Mineral Resources Evaluation in Northeast Asia, Ministry of Land and Resources of China, Changchun, 130061, China

Correspondence to: Wen Liang Xu (xuwl@jlu.edu.cn)

Abstract. To investigate the timing of deposition and provenance of early Mesozoic strata in the northeastern North China Craton (NCC), and to understand the early Mesozoic paleotectonic evolution of the region, we combine stratigraphy, U–Pb zircon geochronology, and Hf isotopic analyses. Early Mesozoic strata include the Early Triassic Heisonggou, Late Triassic Changbai and Xiaoyingzi, and Early Jurassic Yihe formations. Detrital zircons in the Heisonggou Formation yield ~58 % Neoarchean to Paleoproterozoic ages and ~42 % Phanerozoic ages, and were sourced from areas to the south and north of the basins within the NCC, respectively. This indicates that Early Triassic deposition was controlled primarily by the southward subduction of the Paleo-Asian oceanic plate beneath the NCC and collision between the NCC and the Yangtze Craton (YC). Approximately 88 % of the sediments within the Late Triassic Xiaoyingzi Formation were sourced from the NCC to the south, with the remaining ~12 % from the Xing'an–Mongolia Orogenic Belt (XMOB) to the north. This implies that Late Triassic deposition was related to the final closure of the Paleo-Asian Ocean during the Middle Triassic and the rapid exhumation of the Su–Lu Orogenic Belt between the NCC and YC. In contrast, ~88 % of sediments within the Early Jurassic Yihe Formation were sourced from the XMOB to the north, with the remaining ~12 % from the NCC to the south. We therefore infer that rapid uplift of the XMOB and the onset of subduction of the Paleo-Pacific Plate beneath Eurasia occurred in the Early Jurassic.

1 Introduction

The Mesozoic tectonic evolution of the East Asian continental margin has been commonly interpreted as a response to multiple and overprinting tectonic event, commonly referred to as (i) the closure of the Paleo-Asian Ocean (Sengör and Natal'in, 1996; Li, 2006; Zhang et al., 2009, 2010, 2014; Zhou et al., 2010, 2015; Tang et al., 2013; Xu et al., 2013, 2014, 2015; Zhao et al., 2017), (ii) the subduction of the Paleo-Pacific Plate (Lin et al., 1998; Li et al., 1999; Wu et al., 2000, 2004, 2007b; Jia et al., 2004; Zhang et al., 2004; Shen et al., 2006; Xu et al., 2009, 2013), and (iii) subduction and collision between the North China Craton (NCC) and the Yangtze Craton (YC) (Yang et al., 2007; Pei

et al., 2008). Within such tectonic scenarios, the northeastern NCC (as a component of the East Asian continental margin; Fig. 1) is a key area for deciphering the spatio-temporal Mesozoic tectonic evolution at a regional scale.

Two main aspects are still debated in the literature regarding the Mesozoic tectonic evolution of the northeastern NCC: (1) the timing of final closure of the Paleo-Asian Ocean, and (2) the timing of onset of subduction of the Paleo-Pacific Plate beneath Eurasia. Up to now, various opinions exist regarding the closure of the Paleo-Asian Ocean, referred to the Late Permian (JBGMR, 1988; Shi, 2006), Early–Middle Permian to Middle Triassic (Wang et al., 2015b), and Early–Middle Triassic (Sun et al., 2004; Li et al., 2007; Cao et al., 2013), respectively. Similarly, regarding the timing of subduction onset of the Paleo-Pacific Plate beneath Eurasia, multiple time windows have been proposed so far, including the Early Permian (Ernst et al., 2007; Sun et al., 2015; Yang et al., 2015b; Bi et al., 2016), Late Triassic (Wu et al., 2011; Wilde and Zhou, 2015), latest Triassic to Early Jurassic (Zhou and Li, 2017), and Early Jurassic (Xu et al., 2012, 2013; Guo, 2016; Tang et al., 2016; Wang et al., 2017). These contrasting reconstructions were mainly derived from studies of the Mesozoic igneous rocks (especially granitoids) in northeastern China (Li et al., 1999; Wu et al., 2002, 2007a, 2007b; Ge et al., 2007; Zhao and Zhang, 2011; Xu et al., 2012, 2013; Dong et al., 2014, 2016; Yang et al., 2015a, 2015b, 2016).

Basin stratigraphy and sedimentary provenance studies may provide direct supplementary (and possibly alternative) evidence for reconstructing the regional tectonic and paleogeographic evolution during early Mesozoic. Some examples on reconstructing the paleotectonic setting by studying the evolution of sedimentary basins have been carried out in the northern and western–central NCC (Meng, 2003; Meng et al., 2011, 2014; Li and Huang, 2013; Li et al., 2015; Liu et al., 2015; Xu et al., 2016; Meng, 2017), but the formation timing, evolution, and tectonic setting of the early Mesozoic strata in the northeastern NCC remain poorly constrained.

The northeastern NCC contains a series of early Mesozoic faulted basins (referred to as the Fusong–Changbai Basin Group; JBGMR, 1976; Fig. 1) that are filled by volcanics and coal-bearing clastic sediments. The sedimentary from this basins has the potential to decode the tectonic evolution of the northeastern NCC in the frame of the Mesozoic regional geodynamic scenario.

The establishment of the Mesozoic stratigraphic framework of the northeastern NCC is based primarily on lithostratigraphic correlation (JBGMR, 1963, 1976, 1988, 1997). The lack of precise age data has resulted in some uncertainties regarding the sedimentary strata in the northeastern NCC, including (1) the timing of deposition; (2) the lithostratigraphic framework; (3) the sediment source for the basins; and (4) the relationship between basin evolution and the regional tectonic setting.

In this contribution, we focus on the sedimentary strata from the basins in the northeastern NCC (Figs. 1–2) and use U–Pb geochronology and Hf isotopic systematics from detrital and magmatic zircons, combined with available biostratigraphic data to constrain the timing of deposition and the provenance of the early Mesozoic strata, and to

establish a new stratigraphic framework for the northeastern NCC. Provenance analysis provides new insights into the paleotectonic evolution and reveals the early Mesozoic evolution of multiple tectonic regimes in the northeastern NCC.

2 Geological background

The study area is located in the northeastern NCC at the intersection between three main tectonic domains (Fig. 1): the eastern Central Asian Orogenic Belt (CAOB) to the north, and the Su–Lu Orogenic Belt to the south, and the Paleo-Pacific Orogen to the east. The eastern CAOB, which is also referred to as the Xing'an–Mongolia Orogenic Belt (XMOB), consists of a collage of microcontinental massifs, which are (from southeast to northwest) the Khanka, Jiamusi, Songnen–Zhangguangcai Range, Xing'an, and Erguna massifs (Sengör and Natal'in, 1996; Li et al., 1999; Jahn et al., 2004; Li, 2006; Fig. 1). The Su–Lu Orogenic Belt and its eastward extension, the Jing–Ji Orogenic Belt (JJOB) in Korea, formed during the early Mesozoic subduction and collision between the NCC and YC.

The tectonic evolution of the northeastern NCC is characterized by early Paleozoic arc–continent collision (Pei et al., 2014), late Paleozoic subduction of the Paleo-Asian oceanic plate beneath the NCC (Cao et al., 2012), and Middle–Late Permian to Middle Triassic closure of the Paleo-Asian Ocean (Sun et al., 2004; Li et al., 2009a; Wang et al., 2015b). During the early Mesozoic, the northeastern NCC was influenced by subduction, collision, and subsequent rapid exhumation between the NCC and YC (Zheng et al., 2003; Yang et al., 2007; Pei et al., 2008; Liu et al., 2009). Subduction of the Paleo-Pacific Plate beneath Eurasia controlled the Mesozoic tectonic evolution of the East Asian continental margin (Xu et al., 2013). The Dunhua–Mishan and Yitong–Yilan faults occur in the northwestern part of the study area.

The northeastern NCC is composed primarily of Archean and Paleoproterozoic metamorphic basement (including the An'shan, Ji'an, and Laoling groups), Neoproterozoic and Paleozoic sedimentary cover sequences, and several Mesozoic basins (referred to as the Fusong–Changbai Basin Group) (Fig. 1). Neoproterozoic strata comprise sandstone and limestone with minor stromatolites. Cambrian–Middle Ordovician strata are mainly epicontinental carbonate sediments, whereas Late Carboniferous to early Permian units are characterized by marine and coal-bearing terrestrial sequences that are unconformably overlain by Mesozoic volcano-sedimentary formations. The region lacks Silurian–Devonian and Early Carboniferous strata due to uplift of the craton during the middle Paleozoic (SBGMR, 1989). Cenozoic basalts are common in the eastern part of the study area (JBGMR, 1988, 1997; Fig. 2).

The interior of the NCC contains widespread Neoarchean to Paleoproterozoic magmatic rocks (Wu et al., 2007b), but lacks evidence of late Neoproterozoic or Paleozoic magmatism (except for early Paleozoic kimberlite) (JBGMR, 1988; LBGMR, 1989; IMBGMR, 1991). However, the northern margin of the NCC contains abundant Paleozoic igneous rocks (Zhang et al., 2004, 2010; Cao et al., 2013; Pei et al., 2016). In the northeastern NCC, Paleozoic igneous rocks are concentrated to the north of the study area and are characterized by negative (−20 to −2) and positive (0 to +17, with minor −2 to 0) $\varepsilon_{Hf}(t)$ values within the NCC and XMOB (Yang et al., 2006), respectively. The northern NCC contains Ordovician (467 Ma, dated by laser ablation–inductively coupled plasma–mass spectrometry, LA–ICP–MS) medium-K calc-alkaline

pyroxene andesites and Middle Permian (270 Ma, LA–ICP–MS) garnet-bearing monzogranites with zircon $\varepsilon_{Hf}(t)$ values of –5.96 to –2.43 (Pei et al., 2016) and –17.1 to –14.1 (Cao et al., 2013), respectively. In contrast, the XMOB contains Late Cambrian (493 Ma, LA–ICP–MS) low-K tholeiitic meta-diabase and Late Permian (260 Ma, LA–ICP–MS) biotite monzogranite that yield zircon $\varepsilon_{Hf}(t)$ values of +9.42 to +14.89 (Pei et al., 2016) and +8.31 to +9.80 (Wang et al., 2015b), respectively.

Mesozoic magmatism was widespread along the East Asian continental margin (including the northeastern NCC and eastern XMOB). Within the northeastern NCC, Mesozoic magmatism occurred during the Late Triassic, Early Jurassic, Late Jurassic, Early Cretaceous, and Late Cretaceous (Yu et al., 2009; Xu et al., 2013; Zhang et al., 2014; Wang et al., 2017). Mesozoic igneous rocks in the NCC and XMOB yield negative (–20 to –2) and positive (0 to +17, with few values of –2 to 0) zircon $\varepsilon_{Hf}(t)$ values (Yang et al., 2006; Pei et al., 2008; Wang et al., 2015b), respectively.

Mesozoic strata are well preserved and exposed in the study area, and are characterized by coal-bearing volcano-sedimentary formations containing abundant animal and plant fossils. Studies of Mesozoic strata in the northeastern NCC and the establishment of their lithostratigraphic sequence began during geological surveying in the 1960s–1970s. These strata were then reclassified and a general lithostratigraphic sequence was established by JBGMR (1997). Early Mesozoic strata in the study area include, from bottom to top, the Heisonggou, Changbai, Xiaoyingzi, and Yihe formations (Fig. 3). However, the timing of deposition and the stratigraphic sequence of these Triassic–Early Jurassic formations are based mainly on lithostratigraphic correlations and remain debated. The Fusong–Changbai Basin Group represents a series of small- to medium-sized basins in the northeastern NCC. In this study, we focus on three small basins (from north to south): the Fusong, Yihe, and Yantonggou basins (Figs. 2–3). The Fusong Basin is located around Songshu Village and is filled by the Late Triassic Xiaoyingzi Formation ("Formation" is hereafter abbreviated to "Fm"), which is overlain by the Early Cretaceous Guosong Fm. The Yihe Basin, located around Yihe Village, is filled by the Late Triassic Changbai and Early Jurassic Yihe Formations. The Yantonggou Basin is located around Heisonggou Village and is filled by the Early Triassic Heisonggou Fm. These strata represent the early Mesozoic sedimentary sequence of the Fusong–Changbai Basin Group, and record deposition controlled by the tectonics of the northeastern NCC. The lithostratigraphic units are described in detail below (Fig. 3).

The Heisonggou Formation comprises conglomerate, sandstone, siltstone, and shale, and contains plant fossils. The stratotype is exposed in Heisonggou Village, strikes E–W, and extends westward into Korea (Fig. 2, section 3). The stratotype displays faulted contacts with the under- and overlying Mesoproterozoic strata (JBGMR, 1963, 1976). The basal conglomerate contains clasts of quartzite, marble, phyllite, and schist derived from the underlying Mesoproterozoic units. Sandstone, siltstone, and shale are concentrated within the middle and upper strata. The upper part of the section is intruded by andesites (Fig. 4).

The Changbai Formation comprises a lower member of andesites and andesitic volcaniclastics, and an upper member of rhyolite and rhyolitic volcaniclastics. The stratotype is located in Naozhi Village. The formation overlies Paleoproterozoic strata with a faulted contact, and is unconformably overlain by the Early Jurassic Yihe Fm (JBGMR, 1997). The formation strikes E–

W and is also observed in Naozhi and Yihe villages (Fig. 2, section 2).

The Xiaoyingzi Formation comprises a ~30-m-thick lower member of conglomerate and sandstone (representing a complete depositional cycle) and an upper member of sandstone, siltstone, shale, mudstone, and coal. The conglomerate contains clasts of stromatolite-bearing dolomite that were sourced primarily from Neoproterozoic units. Diabase porphyrite commonly intrudes along bedding planes. A thin layer of tuffaceous siltstone occurs in the middle of the section, and abundant plant and animal fossils are preserved within the middle and upper parts of the formation (Fig. 5). Volcanics and organic-rich beds have been used to constrain the age of the Xiaoyingzi Fm. The stratotype is exposed in Xiaoyingzi Village and the strata strike NW–SE (Fig. 2, section 1). The base of the section is not exposed and the formation is overlain by Early Cretaceous volcanics of the Guosong Fm (JBGMR, 1963, 1976; Fig. 5).

The Yihe Formation comprises dominantly conglomerate, sandstone, siltstone, shale, coal, and minor tuffaceous siltstone (JBGMR, 1976, 1997, 1998; Fig. 6). It unconformably overlies andesites of the Late Triassic Changbai Fm, which is present as gravels within the basal conglomerate of the Yihe Fm, thereby illustrating a conformable relationship between the two formations. The stratotype is exposed in Yihe Village and the strata strike E–W (Fig. 2, section 2).

3 Materials and Methods

The Fusong–Changbai Basin Group studied here is chosen from a series of early Mesozoic faulted basins in the northeastern NCC. Three stratotypes of the early Mesozoic sedimentary strata were studied, which are exposed in Xiaoyingzi (Xiaoyingzi Fm: 42°01’54.26” N, 127°10’03.89” E), Naozhi (Yihe Fm: 41°56’41.17” N, 127°04’05.67” E), and Heisonggou (Heisonggou Fm: 41°47’34.79” N, 126°58’33.10” E) villages (see section 2 for further details).

Stratigraphic logs and zircon (detrital and magmatic as recovered from volcanic strata) U–Pb geochronology and Hf isotopic systematics are used to study the age and provenance of the sedimentary strata. The research rationale is based on the following steps: (1) the stratotypes were measured in the field to understand the lithostratigraphic succession and to guide the sampling; (2) detrital and magmatic zircon geochronological data, combined with biostratigraphic data from previous studies, and stratigraphic correlation are used to establish a new stratigraphic framework for the northeastern NCC; (3) detrital zircon age distributions and Hf isotopic compositions are used to identify the source of sedimentary strata and (4) based on provenance data, we reconstruct and discuss the paleogeography and evolution of multiple tectonic regimes in the northeastern NCC.

3.1 Sample descriptions

For zircon U–Pb dating, we collected detrital and magmatic zircons from 10 early Mesozoic sandstone and igneous samples (Fig. 3). Three samples were collected from the Heisonggou Fm, one from the Changbai Fm, three from the Xiaoyingzi Fm, two from the Yihe Fm, and one from the Guosong Fm, which overlies the Xiaoyingzi Fm. Details of their stratigraphy and petrography are presented in Figures 4–7 and described below.

Sample 16LJ6-1 is a medium-grained feldspathic quartz sandstone from the lower Heisonggou Fm (Fig. 4). The sample

is gray–white in color, displays clastic texture, and shows bedded structure. Grains are 0.3–0.6 mm in size and comprise plagioclase and alkali-feldspar (~14 vol. %), quartz (~78 vol. %), lithic fragments (~2 vol. %), and matrix (~5 vol. %) (Fig. 7a).

Sample 15LJ4-11 is a fine-grained feldspathic quartz sandstone from the upper Heisonggou Fm. The sample is gray–white in color, exhibits clastic texture, and shows bedded structure. Grains are angular–subangular and 0.1–0.2 mm in size, comprising plagioclase and alkali-feldspar (~13 vol. %), quartz (~78 vol. %), lithic fragments (~2 vol. %), and calcareous cement (~6 vol. %) (Fig. 7b).

Sample 15LJ4-6 is an andesite that intrudes the Heisonggou Fm (Fig. 4). It is light gray–green in color, displays pilotaxitic texture, and shows massive structure (Fig. 7c).

Sample 15JFS1-1 is a medium-grained feldspathic quartz sandstone from the lower Xiaoyingzi Fm (Fig. 5). It is yellow–white in color, displays clastic texture, and shows bedded structure. Grains are 0.4–0.8 mm in size and comprise quartz (~80 vol. %), plagioclase and alkali-feldspar (~12 vol. %), lithic fragments (~3 vol. %, volcanic fragments), and matrix (~4 vol. %) (Fig. 7d).

Sample 15JFS2-1 was collected from a diabase porphyrite intruding the Xiaoyingzi Fm (Fig. 5). It is gray–green in color, displays porphyritic texture, and shows massive structure. The phenocrysts are dominantly plagioclase (~5 vol. %) and the groundmass displays pilotaxitic texture (Fig. 7e).

Sample 16LJ8-1 is a tuffaceous siltstone from the middle Xiaoyingzi Fm (Fig. 5). The sample is white in color, displays clastic texture, and shows bedded structure.

Sample 15JFS10-1 is a pyroxene andesite that unconformably overlies the Xiaoyingzi Fm. (Fig. 5). The andesite belongs to the Guosong Fm and is gray–green in color, displays porphyritic texture, and shows massive structure (Fig. 7f).

Sample 16LJ1-1 is an andesite from the Changbai Fm, which underlies the Yihe Fm. The andesite is gray–green in color, displays porphyritic texture, and shows massive structure. The phenocrysts are mainly plagioclase (~10 vol. %) and the groundmass exhibits pilotaxitic texture (Fig. 7g).

Sample 15LJ1-2 is a fine-grained feldspathic quartz sandstone from the middle Yihe Fm (Fig. 6). It is gray–white in color, displays clastic texture, and shows bedded structure. The rock comprises plagioclase and alkali-feldspar (~13 vol. %), quartz (~78 vol. %), lithic fragments (~3 vol. %), and matrix (~5 vol. %).

Sample16LJ3-1 is a tuffaceous siltstone from the upper Yihe Fm. It is white in color, displays clastic texture, and shows bedded structure (Fig. 7h).

3.2 Analytical methods

3.2.1 Zircon U–Pb dating

Zircons were separated from samples using conventional heavy liquid and magnetic techniques, and purified by handpicking under a binocular microscope at the Langfang Yantuo Geological Survey, Langfang, Hebei Province, China. The handpicked zircons were examined under transmitted and reflected-light using an optical microscope, and

cathodoluminescence (CL) images were obtained to reveal their internal structures, using a JEOL scanning electron microscope housed at the State Key Laboratory of Continental Dynamics, Northwest University, Xi'an China. Based on CL images, distinct domains within the zircons were selected for analysis. An Agilent 7500a ICP–MS equipped with a 193 nm laser, housed at the State Key Laboratory of Geological Processes and Mineral Resources, China University of Geosciences, Wuhan, China, was used to measure the U–Pb ages of zircons. Zircon 91500 was used as external standard for age calibration and the NIST SRM 610 silicate glass was used for instrument optimization. The spot diameter was 32 μm. For details of the instrumental parameters and procedures, see Yuan et al. (2004). The ICPMSDataCal 7.0 (Liu et al., 2010) and Isoplot 3.0 (Ludwig, 2003) programs were used for data analysis and plotting. Correction for common Pb was made following Andersen (2002). Errors on individual LA–ICP–MS analyses are quoted at the 1σ level, while errors on pooled ages are quoted at the 95 % (2σ) confidence level. The dating results are presented in Table S1.

Due to the paucity of zircons recovered from samples 15JFS2-1 (diabase porphyrite) and 15JFS10-1 (pyroxene andesite), analysis of these two samples was conducted using a Cameca 1280 secondary ion mass spectrometer (SIMS) at the Institute of Geology and Geophysics, Chinese Academy of Sciences, Beijing, China, using operating and data processing procedures similar to those described by Li et al. (2009b).

3.2.2 Hf isotopic analyses

In situ zircon Hf isotope analyses were conducted using a Neptune Plus multi-collector (MC)–ICP–MS (Thermo Fisher Scientific, Germany) equipped with a 193 nm excimer ArF laser ablation system (Lambda Physik, Göttingen, Germany) at the State Key Laboratory of Geological Processes and Mineral Resources, China University of Geosciences. Laser ablation analyses used an energy density of 5.3 J cm^{-2}. Helium was used as the carrier gas within the ablation cell and was merged with argon (makeup gas) after the ablation cell. A simple Y-junction downstream from the sample was used to add small amounts of nitrogen (4 ml min^{-1}) to the argon makeup gas flow (Hu et al., 2008a, 2008b). Compared with the standard arrangement, the addition of nitrogen, in combination with the use of a newly designed X skimmer and Jet sample cones in the Neptune Plus instrument, improved the signal intensities of Hf, Yb, and Lu by factors of 5.3, 4.0, and 2.4, respectively. All data were acquired in single-spot ablation mode with a 44 μm spot size. Each measurement consisted of 20 s of acquisition of the background signal followed by 50 s of ablation signal acquisition. For further details of the operating conditions for the laser ablation system and the MC–ICP–MS instrument, and analytical procedures followed, see Hu et al. (2012). The dating results are presented in Table S2.

4 Analytical results

4.1 Zircon U–Pb dating

4.1.1 Heisonggou Formation

Zircons from sample 16LJ6-1 are euhedral–subhedral, display fine oscillatory growth zoning in cathodoluminescence (CL) images (Fig. 8a), and yield Th/U values of 0.07–1.31, indicating a magmatic origin (Corfu et al., 2003). A total of 68 spots provide ages ranging from 2485 to 248 Ma (ages of >1000 Ma use $^{207}Pb/^{206}Pb$ ages, whereas ages of <1000 Ma use $^{206}Pb/^{238}U$ ages), yielding four major age populations with weighted-mean ages of 252 ± 1 Ma (MSWD = 1, n = 21), 293 ± 2 Ma (MSWD = 1.2, n = 10), 323 ± 2 Ma (MSWD = 0.39, n = 15), and 2402 ± 12 Ma (MSWD = 8.5, n = 14) (Fig. 9a). Other grains yield ages of 339 (2 grains), 594, 1757, 1791, 2006, 2075, and 2171 Ma (Table S1). The youngest zircon age population of 252 ± 1 Ma constrains the maximum depositional age of this sample (i.e., the medium-grained feldspathic quartz sandstone was deposited after ~252 Ma).

Zircon grains from sample 15LJ4-11 are euhedral–subhedral, display fine oscillatory growth zoning in CL images (Fig. 8b), and yield Th/U values of 0.01–4.31. Some grains are round in shape and exhibit a core–rim texture. A total of 72 spots provide ages ranging from 2832 to 248 Ma and nine age populations with weighted-mean ages of 253 ± 3 Ma (MSWD = 0.4, n = 7), 270 ± 3 Ma (MSWD = 0.24, n = 7), 304 ± 3 Ma (MSWD = 0.38, n = 5), 323 ± 3 Ma (MSWD = 0.12, n = 6), 360 ± 5 Ma (MSWD = 0.35, n = 3), 382 ± 7 Ma (MSWD = 0.03, n = 3), 1845 ± 9 Ma (MSWD = 1.7, n = 14), 2337 ± 23 Ma (MSWD = 4.8, n = 4), and 2504 ± 8 Ma (MSWD = 4.0, n = 20) (Fig. 9b). Other grains yield ages of 426, 2152, and 2838 Ma (Table S1). The youngest zircon age population of 253 ± 3 Ma represents the maximum depositional age of the fine-grained feldspathic quartz sandstone.

Zircons from sample 15LJ4-6 are euhedral–subhedral and display fine oscillatory growth zoning in CL images (Fig. 8c), with Th/U values of 0.07–1.03. A total of 20 spots provide ages ranging from 2435 to 243 Ma, with two age populations with weighted-mean ages of 246 ± 2 Ma (MSWD = 1.6, n = 8) and 297 ± 3 Ma (MSWD = 2.2, n = 6) (Fig. 9c). Other grains yield ages of 268, 313, 1788, 1819, 2411, and 2435 Ma (Table S1). The mean age of 246 ± 2 Ma is interpreted as the crystallization age of the andesite, whereas the other ages are interpreted as captured zircons.

4.1.2 Changbai Formation

Zircon grains from the andesite (sample 16LJ1-1) are euhedral–subhedral and display typical oscillatory growth zoning in CL images (Fig. 8d), with Th/U values of 0.46–1.06. Twenty-five analyses yield a weighted-mean $^{206}Pb/^{238}U$ age of 227 ± 1 Ma (MSWD = 0.74, n = 25) (Fig. 9d; Table S1), which is interpreted as the crystallization age of the andesite.

4.1.3 Xiaoyingzi Formation

Zircons from sample 15JFS1-1 are euhedral–subhedral and show fine oscillatory growth zoning in CL images, with Th/U values of 0.05–1.58. Some rare grains are rounded in shape and display fine oscillatory zoning in CL images (Fig. 8e).

A total of 79 spots provide ages ranging from 3285 to 220 Ma, yielding five age populations with weighted-mean ages of 224 ± 3 Ma (MSWD = 0.39, n = 7), 232 ± 5 Ma (MSWD = 0.27, n = 3), 257 ± 5 Ma (MSWD = 2.3, n = 3), 1880 ± 3 Ma (MSWD = 2.9, n = 42), and 1982 ± 21 Ma (MSWD = 1.2, n = 4) (Fig. 9e). Other grains yield ages of 275, 277, 294, 296, 315, 364, 369, 392, 397, 433, 453, 496, 569, 691, 708, 1768, 2242, 2434, 2500, and 3285 Ma (Table S1). The youngest zircon age population of 224 ± 3 Ma constrains the maximum depositional age of the medium-grained feldspathic quartz sandstone.

Zircons from the diabase porphyrite (sample 15JFS2-1) are euhedral–subhedral and display mainly oscillatory growth zoning, although some grains exhibit core–rim structures (Fig. 8f). A total of 17 spots provide ages ranging from 2516 to 111 Ma, with a peak zircon age population at 113 ± 2 Ma (MSWD = 3.4, n = 5) (Fig. 9f). Other grains yield ages of 173, 218, 270, 332, 744, 1862, 1884, 1887, 1891, 2059, 2412, and 2516 Ma (Table S1). The youngest weighted-mean $^{206}Pb/^{238}U$ age of 113 ± 2 Ma is considered to represent the age of intrusion of the diabase porphyrite.

Zircon grains from the tuffaceous siltstone (sample 16LJ8-1) are typically euhedral–subhedral and display oscillatory growth zoning in CL images, although some grains are rounded or subrounded (Fig. 8g). Zircons yield Th/U values of 0.04–1.2. A total of 65 spots provide ages ranging from 2602 to 223 Ma, defining six zircon age populations with weighted-mean ages of 227 ± 2 Ma (MSWD = 4.1, n = 3), 259 ± 2 Ma (MSWD = 4.5, n = 5), 1770 ± 9 Ma (MSWD = 1.9, n = 18), 1831 ± 9 Ma (MSWD = 2.1, n = 16), 2212 ± 18 Ma (MSWD = 7.7, n = 5), and 2486 ± 15 Ma (MSWD = 8.3, n = 7) (Fig. 9g). Other grains yield ages of 240 (two grains), 316, 330, 505, 914, 1469, 1950, 2023, 2061, and 2602 Ma (Table S1). The youngest $^{206}Pb/^{238}U$ age of 223 ± 2 Ma is interpreted as the maximum depositional age of the tuffaceous siltstone.

4.1.4 Yihe Formation

Zircon grains from sample 15LJ1-2 are primarily euhedral–subhedral and display fine oscillatory zoning in CL images, whereas other grains are rounded and display oscillatory zoning (Fig. 8h), which, together with their Th/U values of 0.11–1.72, indicates a magmatic origin (Table S1). A total of 77 spots provide ages ranging from 2472 to 177 Ma, yielding six zircon age populations with weighted-mean ages of 184 ± 2 Ma (MSWD = 1.7, n = 7), 233 ± 3 Ma (MSWD = 0.82, n = 7), 245 ± 1 Ma (MSWD = 1.17, n = 17), 254 ± 2 Ma (MSWD = 0.72, n = 20), 266 ± 2 Ma (MSWD = 1, n = 11), and 1831 ± 17 Ma (MSWD = 9.9, n = 4) (Fig. 9h). Other grains yield ages of 191, 200, 211, 286, 293, 323, 363, 460, 1468, 2471, and 2472 Ma (Table S1). These results indicate that the fine-grained feldspathic quartz sandstone was deposited after 184 Ma.

Zircon grains from sample 16LJ3-1 are typically euhedral–subhedral and display fine oscillatory growth zoning in CL images (Fig. 8i), which, together with their Th/U values of 0.26–1.16, are indicative of a magmatic origin. A total of 65 spots provide ages ranging from 2477 to 178 Ma, yielding three zircon age populations with weighted-mean ages of 182 ± 1 Ma (MSWD = 3.3, n = 20), 253 ± 1 Ma (MSWD = 0.74, n = 33), and 1831 ± 20 Ma (MSWD = 1.8, n = 4) (Fig. 9i). Other grains yield ages of 212, 222, 237, 263, 276, 340, 2457, and 2477 Ma (Table S1). The youngest age population of 182 ± 1 Ma represents the maximum depositional age of the tuffaceous siltstone.

4.1.5 Guosong Formation

Zircon grains from the pyroxene andesite (15JFS10-1) are euhedral–subhedral and display oscillatory growth zoning and striped absorption in CL images (Fig. 8j), with Th/U values of 0.19–2.05. A total of 14 spots provide ages ranging from 1647 to 112 Ma, defining two zircon age populations with weighted-mean ages of 113 ± 3 Ma (MSWD = 1.19, n = 2) and 227 ± 3 Ma (MSWD = 0.74, n = 7) (Fig. 9j). Other grains yield ages of 156, 425, 438, 946, and 1647 Ma (Table S1). The youngest age of 113 ± 3 Ma is interpreted as the crystallization age of the pyroxene andesite.

4.2 Zircon Hf isotopes

We performed *in situ* Hf isotopic analysis on the same spots as used for U–Pb dating on samples from the Heisonggou (15LJ4-11), Xiaoyingzi (15JFS1-1), and Yihe (15LJ1-2) formations. The results are listed in Table S2 and shown in Fig. 10.

4.2.1 Heisonggou Formation

We determined the Hf isotopic compositions of 22 detrital zircons from the Heisonggou Fm. Three zircon grains (~13.6 %) with ages of 2513–2466 Ma yielded $\varepsilon_{Hf}(t)$ values of –4.2 to +4.9, four Paleoproterozoic (1862–1812 Ma) grains (~18.2 %) yielded $\varepsilon_{Hf}(t)$ values of –1.9 to +0.2, and fifteen Phanerozoic (383–250 Ma) grains (~68.2 %) yielded $\varepsilon_{Hf}(t)$ values of –16.3 to –7.0 (Table S2; Fig. 10a) and two-stage model (T_{DM2}) ages of 2.3–1.7 Ga, similar to zircons from Phanerozoic igneous rocks in the NCC (Yang et al., 2006).

4.2.2 Xiaoyingzi Formation

We determined the Hf isotopic compositions of 25 detrital zircons with ages of 1928–221 Ma from the Xiaoyingzi Fm. Most zircon grains (~88 %) yielded negative $\varepsilon_{Hf}(t)$ values of –21.9 to –0.2 and T_{DM2} ages of 2.7–1.6 Ga, whereas three zircon grains (~12 %) with ages of 569, 496, and 453 Ma yielded positive $\varepsilon_{Hf}(t)$ values of +2.9 to +8.5 and T_{DM2} ages of 1.2–0.98 Ga (Table S2; Fig. 10b). Two grains within the latter, with ages of 708 and 691 Ma, yielded $\varepsilon_{Hf}(t)$ values of –10.9 and –6.1 and T_{DM2} ages of 2.3 and 2.0 Ga, respectively.

4.2.3 Yihe Formation

We determined the Hf isotopic compositions of 17 detrital zircons with ages of 255–177 Ma from the Yihe Fm. Most grains (~88 %) yielded positive $\varepsilon_{Hf}(t)$ values of +2.4 to +12.6 and T_{DM2} ages of 1.1–0.4 Ga, whereas two zircon grains (~12 %) with ages of 248 Ma yielded negative $\varepsilon_{Hf}(t)$ values of –5.8 and –1.9 and T_{DM2} ages of 1.6 and 1.4 Ga (Table S2; Fig. 10c).

5 Discussion

5.1 Age of early Mesozoic strata in the northeastern NCC

Here we combine the ages of youngest concordant detrital zircons, interbedded volcanic and intrusive rocks, and overlying

strata, as well as the available biostratigraphic data, to constrain the ages of Mesozoic strata in the northeastern NCC.

5.1.1 Heisonggou Formation

The Heisougou Fm was first defined in Heisonggou Village and was assigned to the Early Jurassic (JBGMR, 1963). It was subsequently reclassified as the Shiren Fm and assigned to the Early Cretaceous (JBGMR, 1997). Therefore, the age of the Heisonggou Fm remains uncertain. In this study, samples from the lower (16LJ6-1) and upper (15LJ4-11) Heisonggou Fm yield youngest zircon age populations of 252 ± 1 Ma and 253 ± 3 Ma, respectively, indicating that deposition of the Heisonggou Fm occurred after 252 ± 1 Ma. Furthermore, andesite intruding this unit (Fig. 4, sample 15LJ4-6) yields a weighted-mean age of 246 ± 2 Ma, thereby constraining the deposition of the Heisonggou Fm to between 252 and 246 Ma. This Early Triassic age contrasts with the previously proposed Early Jurassic (JBGMR, 1963) and Early Cretaceous (JBGMR, 1997) ages.

5.1.2 Changbai Formation

The Changbai Fm was first defined in Caiyuanzi and Ergulazi villages and was assigned to the Late Triassic. The formation comprises intermediate–acidic volcanics and has been reassigned into the Ergulazi and Naozhigou formations (JBGMR, 1976, 1997). Zircon U–Pb dating of andesite (16LJ1-1) from the Changbai Fm yielded a weighted-mean age of 227 ± 1 Ma. Combined with a previously reported zircon $^{206}Pb/^{238}U$ age of 222 ± 1 Ma (Yu et al., 2009) from the Naozhigou Fm in the northern area of Caiyuanzi Village, we confirm that the Changbai Fm was deposited in the Late Triassic.

5.1.3 Xiaoyingzi Formation

The Xiaoyingzi Fm was first defined in Hengdaohezi and Xiaoyingzi villages and assigned to the Early Jurassic (JBGMR, 1971). It was later correlated with the Xiaohekou Fm and assigned to the Late Triassic (JBGMR, 1988, 1997). In contrast, JBGMR (2007) classified placed within the Yihe Fm and assigned an Early Jurassic age. Thus, the age of the Xiaoyingzi Fm remains controversial. Detrital zircon grains from the medium-grained feldspathic quartz sandstone (15JFS1-1) and tuffaceous siltstone (16LJ8-1) yielded youngest concordant ages of 224 ± 2 Ma and 223 ± 2 Ma, respectively, indicating that the Xiaoyingzi Fm was deposited after ~223 Ma. Freshwater bivalve fossils (e.g., *Ferganoconcha* sp. and *Sibireconcha* sp.) in this formation belong to the *Unio–Shaanxiconcha* assemblage (Zhu, 1991; JBGMR, 1997), which is similar to assemblages found in Late Triassic strata in China, South Australia, North American, and South Africa (Zhu, 1991). Plant fossil assemblages (e.g., *Glossophyllum–Neocalamites*) in this formation are generally limited to the Late Triassic–Early Jurassic (JBGMR, 1997). We therefore conclude that the Xiaoyingzi Fm was deposited in the Late Triassic. The previously described "interbedded volcanic rocks" within the Xiaoyingzi Fm (JBGMR, 1971) are here reinterpreted as diabase porphyrite (15JFS2-1), which was intruded at 113 ± 2 Ma. Zircon grains from the pyroxene andesite (15JFS10-1) of the Guosong Fm also yield an age of 113 ± 3 Ma. These results indicate that the Guosong Fm, which overlies the Xiaoyingzi Fm, and the diabase porphyrite have similar ages and were produced during coeval magmatism.

5.1.4 Yihe Formation

The Yihe Formation was first defined in Naozhigou and Yihe villages and was assigned to the Early Jurassic (JBGMR, 1976). Previous studies referred to this unit as the Yantonggou and Shiren formations, which were assigned to the Late Jurassic and Early Cretaceous (EGJS, 1975), respectively. Detrital zircon grains from the fine-grained feldspathic quartz sandstone (15LJ1-2) and tuffaceous siltstone (16LJ3-1) yielded youngest age populations of 184 ± 2 Ma and 182 ± 1 Ma, respectively. In addition, Early Jurassic plant fossils such as *Cladophlebis ukienesis*, *Marattia hoerensis*, and *Pterophyllum propinquum* are observed within the Yihe Fm (Si and Zhou, 1962). Based on these observations, combined with the absence of Middle–Late Jurassic strata in southern Jilin Province, we conclude that the Yihe Fm was deposited in the Early Jurassic.

Our new geochronological data, field relationships, and biostratigraphic data are used to establish a new early Mesozoic stratigraphic framework for the northeastern NCC (Fig. 3), which is summarized as follows. The Heisonggou Fm is assigned to the Early Triassic (252–246 Ma) based on the U–Pb ages of detrital and magmatic zircons. The Xiaoyingzi Fm is assigned to the Late Triassic based on zircon geochronological data and fossil assemblages. Deposition of this unit post-dated the Changbai Fm. The Yihe Fm was deposited in the Early Jurassic, consistent with biostratigraphic data (Si and Zhou, 1962).

5.2 Stratigraphic correlation with early Mesozoic strata in the northern NCC

Triassic–Middle Jurassic strata are well preserved and exposed in the northern NCC (Meng, 2017), and were deposited within early Mesozoic basins in the Yinshan–Yanshan Orogenic Belt (e.g., the Beipiao, Xiabancheng, Jingxi, and Shiguaizi basins) (Fig. 11; Meng et al., 2018). The northern NCC shared a similar stratigraphic and sedimentological evolution to the interior of the craton during the Mesoproterozoic to Paleozoic, but has undergone a distinct evolution since the Mesozoic, involving alternating periods of contraction and extension (Davis et al., 2001; Cui et al., 2002).

Triassic–Middle Jurassic deposits in the northern NCC are dominated by volcano-sedimentary formations containing coal and abundant animal and plant fossils, and their stratigraphy, geochronology, and depositional processes are well constrained (Meng, 2003; Meng et al., 2011, 2014; Li and Huang, 2013; Li et al., 2015; Liu et al., 2015; Xu et al., 2016; Meng, 2017). Here, we determine the relationship between early Mesozoic strata in the northern and northeastern NCC.

The Late Permian Tiechang Fm in the northeastern NCC is characterized by gray–purple coarse-grained sandstone, pebbly sandstone, siltstone, and shale, which is a similar lithological association to the Late Permian strata of the northern NCC (e.g., the lower Tiechang Fm correlates with the Shihezi, Naobaogou, and Laowuopu formations; Fig. 11). In contrast, Early Triassic strata (e.g., the Heisonggou Fm) are only observed in the northeastern NCC. In the northern NCC, Middle Triassic strata are rare and only observed within the central area (e.g., the Xiabancheng Basin), and are characterized by sandstone, siltstone, and shale. Such strata are not observed in the northeastern NCC. Late Triassic strata (e.g., the Changbai and Xiaoyingzi formations) are commonly observed in the northeastern NCC, and comprise intermediate–acidic volcanics and coal-bearing clastic sediments. In the northern NCC, coeval and comparable strata are represented by the Xiaolanwuo, Wuchang, and Shanggu formations in the Xiabancheng Basin, as well as the Yangcaogou Fm in the Beipiao Basin. For

example, the Late Triassic Xiaoyingzi Fm in the northeastern NCC contains a similar lithological association and fossil assemblage to the Yangcaogou and Shanggu formations in the northern NCC. Furthermore, ages of volcanics in the Changbai Fm (227 and 222 Ma; Yu et al., 2009) are similar to those of volcanics in the Xiaolanwuo (225 ± 1 Ma) and Wuchang (227.6 ± 2 Ma) (Meng et al., 2018) formations in the Xiabancheng Basin. The Early Jurassic Yihe Fm in the northeastern NCC is comparable to the lower Beipiao, Xiahuayuan, lower Yaopo, and Zhaogou formations in the northern NCC, as indicated by the presence of similar coal-bearing layers and plant fossil assemblages (JBGMR, 1988; HBGMR, 1989; LBGMR, 1989; BBGMR, 1991; IMBGMR, 1991).

In summary, we suggest that similar late Paleozoic sedimentary successions (North China type) occur in both the northern and northeastern NCC. However, Early Triassic strata are only observed within the northeastern NCC. In contrast, Middle Triassic strata are observed within the northern NCC but are absent in the northeastern NCC. Similar Late Triassic sedimentary formations and contemporaneous volcanics are observed in the northern and northeastern NCC. Earliest Jurassic strata are absent in the northern and northeastern NCC, whereas Middle–Late Early Jurassic strata are widespread in both regions, and are correlated based on coal-bearing layers and plant fossils (JBGMR, 1988; HBGMR, 1989; LBGMR, 1989; BBGMR, 1991; IMBGMR, 1991). Furthermore, regional unconformities are identified between Late Permian and Triassic strata, and Late Triassic and Jurassic strata in the northern and northeastern NCC (Fig. 11), respectively.

5.3 Provenance of early Mesozoic strata in the northeastern NCC

A generally accepted method to identify the source of sedimentary units is to compare zircon U–Pb age and Hf isotopic data with areas or units that may have supplied sediment to the region (Dickinson and Gehrels, 2008). Our 502 detrital zircon U–Pb analyses are grouped into three age populations: Neoarchean to Paleoproterozoic, Neoproterozoic, and Phanerozoic (Fig. 12). Magmatic zircon grains from igneous and sedimentary rocks within the northern margin of the NCC generally yield Neoarchean to Paleoproterozoic and late Paleozoic age populations (Yang et al., 2006; Zhang et al., 2010), whereas igneous rocks and Paleozoic sediments from the southern margin of the XMOB contain mainly Phanerozoic and minor Neoproterozoic zircon grains (Meng et al., 2010; Wang et al., 2012, 2014). In addition, Phanerozoic zircons from the NCC typically yield negative $\varepsilon_{Hf}(t)$ values, whereas those from the southern margin of the XMOB typically yield positive $\varepsilon_{Hf}(t)$ values (Yang et al., 2006; Cao et al., 2013). These data are inevitably affected by the sampling strategy, so the given percentage data should be considered qualitatively rather than quantitatively.

5.3.1 Early Triassic Heisonggou Formation

Approximately 58 % of detrital zircon grains from the Early Triassic Heisonggou Fm yield Neoarchean to Paleoproterozoic ages (2.8–1.8 Ga), forming two age peaks at ~2.5 and ~1.8 Ga, which are typical of the NCC (Ma and Wu, 1981; Zhao et al., 2001; Gao et al., 2004). In contrast, the ~42 % magmatic zircon grains yield Phanerozoic ages (426–248 Ma). These Phanerozoic magmatic events are not recorded within the interior of the NCC (Yang et al., 2017), but are instead observed within the northern margin of the NCC (Zhang et al., 2004, 2010; Wu et al., 2011; Cao et al., 2013; Pei et al., 2014;

Wang et al., 2015b, 2016). These observations, combined with the negative $\varepsilon_{Hf}(t)$ values (–16.3 to –7.0) and two-stage model (T_{DM2}) ages of 2.3–1.7 Ga, indicate that all sedimentary material within this formation was sourced from the NCC.

In addition, detrital zircon grains (especially those with Phanerozoic ages) are euhedral–subhedral (with the exception of some rounded Neoarchean and Paleoproterozoic grains), indicating a proximal source. This interpretation is also supported by the short deposition time (between 252 and 246 Ma) of the Heisonggou Fm.

Based on the present distribution of the NCC basement and Phanerozoic igneous rocks in the northeastern NCC (JBGMR, 1988), we suggest that at least 42 % of the sediment was sourced from Phanerozoic igneous rocks along the northern margin of the NCC, to the north of the basin. In contrast, Neoarchean and Paleoproterozoic sediment was likely sourced from regions surrounding the basin.

5.3.2 Late Triassic Xiaoyingzi Formation

Approximately 71 % of detrital zircon grains from the Late Triassic Xiaoyingzi Fm yielded Neoarchean to Paleoproterozoic ages (with peaks at ~2.50 and ~1.88 Ga), indicating that they were sourced from the NCC (Gao et al., 2004). The other analyzed detrital zircon grains yielded ~26 % Phanerozoic (496–220 Ma) and ~3 % Neoproterozoic ages (914–569 Ma). Three zircon grains (with ages of 569, 496, and 453 Ma) yielded positive $\varepsilon_{Hf}(t)$ values (+2.9 to +8.5), whereas the other Phanerozoic and Neoproterozoic grains yielded negative $\varepsilon_{Hf}(t)$ values (–21.9 to –5.0), indicating that the former were sourced from the XMOB and the latter from the NCC (Yang et al., 2006; Cao et al., 2013; Pei et al., 2014).

All Phanerozoic zircons are euhedral–subhedral, suggesting the Xiaoyingzi Fm sediments were not transported over long distances. Combined with the observation of Phanerozoic and minor Neoproterozoic igneous rocks to the north of the basin (JBGMR, 1988), we conclude that ~29 % of sediments from the Xiaoyingzi Fm were sourced from an area to the north of the basin, with the remaining ~71 % sourced from regions surrounding the basin.

5.3.3 Early Jurassic Yihe Formation

Approximately 91 % of detrital zircon grains from the Early Jurassic Yihe Fm yielded Phanerozoic ages (460–177 Ma), with the remaining ~9 % yielding Neoarchean to Paleoproterozoic ages (peaks at ~2.5 and ~1.8 Ga). The former are consistent with Phanerozoic magmatism along the northern margin of the NCC and XMOB, whereas the latter are typical of the NCC interior (Gao et al., 2004; Zhang et al., 2004; Yang et al., 2006; Cao et al., 2013; Wang et al., 2015a). Of the 17 zircon grains analyzed with Phanerozoic ages, two grains (~12 %) with ages of 248 Ma yielded $\varepsilon_{Hf}(t)$ values of –5.8 to –1.9, and the remaining 15 grains (~88 %) yielded $\varepsilon_{Hf}(t)$ values of +2.4 to +12.6. We infer that the former, together with Neoarchean and Paleoproterozoic detrital zircon grains, were sourced from the NCC, whereas the latter were derived from the XMOB (Yang et al., 2006). Furthermore, all Phanerozoic zircon grains are euhedral–subhedral, indicating that the Phanerozoic sediments did not undergo long-distance transport. The age populations and $\varepsilon_{Hf}(t)$ values of the detrital zircon grains indicate that the Yihe Fm was sourced mainly from the XMOB to the north of the basin.

5.4 Implications for the early Mesozoic paleotectonic evolution of the northeastern NCC

The early Mesozoic tectonic evolution of the northeastern NCC was not only influenced by subduction of the Paleo-Asian oceanic plate beneath the NCC and final closure of the Paleo-Asian Ocean to the north (Zhang et al., 2004; Wu et al., 2011; Cao et al., 2013), but also by subduction and collision between the NCC and the YC to the south (Pei et al., 2008, 2011), as well as by subduction of the Paleo-Pacific Plate beneath Eurasia to the east (Xu et al., 2013; Guo, 2016; Wang et al., 2017). However, the spatio-temporal extents of these influences, and the timing of final closure of the Paleo-Asian Ocean and the onset of subduction of the Paleo-Pacific Plate remain controversial (Sun et al., 2004; Shi, 2006; Ernst et al., 2007; Li et al., 2007; Wu et al., 2011; Xu et al., 2012, 2013; Cao et al., 2013; Sun et al., 2015; Wang et al., 2017; Zhou and Li, 2017). Here we use provenance data and interpretations of changes in provenance within early Mesozoic strata of the northeastern NCC to reconstruct the early Mesozoic paleotectonic evolution of the northeastern NCC.

5.4.1 Early Triassic: southward subduction of the Paleo-Asian oceanic plate, and subduction and collision between the NCC and YC

Approximately 42 % of the Early Triassic Heisonggou Fm sediments were sourced from the northern margin of the NCC; there is no evidence of XMOB-sourced grains. We therefore infer that southward subduction of the Paleo-Asian oceanic plate beneath the NCC was ongoing in the Early Triassic (i.e., final closure of the Paleo-Asian Ocean had not yet occurred) (Cao et al., 2013; Wang et al., 2015b). Subduction resulted in uplift along the northern margin of the NCC, producing a paleogeographic highland that acted as a sediment source during deposition of the Heisonggou Fm (Fig. 13a). The remaining ~58 % of sediments of the Heisonggou Fm were sourced from Neoarchean and Paleoproterozoic NCC basement, which is observed in areas surrounding the basin, as well as to the south. We infer that the area to the south of the basin was uplifted in the Early Triassic, consistent with subduction and collision between the NCC and YC at this time (Pei et al., 2008, 2011; Liu et al., 2012; Zheng et al., 2013). Thus, we conclude that southward subduction of the Paleo-Asian oceanic plate and subduction and collision between the NCC and YC resulted in uplift of the northern and southeastern margins of the NCC, respectively. These uplifted highlands provided sediment source areas for the Heisonggou Fm (Figs. 11, 13a).

5.4.2 Late Triassic: final closure of the Paleo-Asian Ocean and post-collisional exhumation of the Su–Lu Orogenic Belt

Zircon Hf isotopic compositions indicate that ~29 % of sediments of the Late Triassic Xiaoyingzi Fm were sourced from areas to the north of the basin (~4 % from the XMOB and ~25 % from the northern margin of the NCC). The presence of XMOB material indicates that the Paleo-Asian Ocean had closed by the Late Triassic. We therefore suggest that final closure of the ocean occurred in the Middle Triassic, which is also supported by the occurrence of Middle Triassic syn-collisional granitoids in the Yanbian region (Wang et al., 2017), as well as the absence of Middle Triassic sedimentary strata in the northeast NCC (JBGMR, 1988). Approximately 71 % of the Xiaoyingzi Fm zircon grains yield Neoarchean and

Paleoproterozoic ages, indicating that they were sourced from the NCC basement. As the NCC basement crops out mainly to the south of the basin, we conclude that this region, which was still a highland at the time, provided the primary source during deposition of the Xiaoyingzi Fm. Furthermore, we suggest that rapid exhumation of ultrahigh-pressure metamorphic rocks within the Su–Lu Orogenic Belt in the Late Triassic (Zhao et al., 2001; Zheng et al., 2013) produced the inferred uplift in the region to the south of the basin (Figs. 11, 13b).

5.4.3 Early Jurassic: rapid uplift of the XMOB and onset of subduction of the Paleo-Pacific Plate beneath Eurasia

The provenance of the Early Jurassic Yihe Fm changed rapidly from ~71 % Neoarchean and Paleoproterozoic basement (the Late Triassic Xiaoyingzi Fm) from an area to the south of the basin in the Late Triassic, to ~91 % Phanerozoic rocks from an area to the north of the basin in the Early Jurassic. In addition, Hf isotopic compositions of Phanerozoic detrital zircon grains indicate that >88 % of the grains were sourced from the XMOB. In other words, these data show that the sediments were sourced mainly from the NCC in the Early–Late Triassic, and mainly from the XMOB in the Early Jurassic. This change in provenance can be directly explained by paleogeographic changes, indicating that rapid uplift of the XMOB occurred during the Early Jurassic (Figs. 11, 13c). In addition, the paleogeographic changes were possibly triggered by a change in tectonic domains, and the uplift in the northeastern NCC might also have been related to the initial subduction of the Paleo-Pacific Plate beneath Eurasia in the Early Jurassic. This interpretation is also supported by the presence of the Early Jurassic accretionary complex and Early Jurassic calc-alkaline igneous rocks in the eastern Asian continental margin. Firstly, the Early Jurassic igneous rocks in the eastern Asian continental margin (including eastern Heilongjiang–Jilin provinces, northeastern North Korea, and south Korea) belong to the calc-alkaline series (Xu et al., 2013; Guo et al., 2016; Wang et al., 2017; Tang et al., 2018; Fig. 1), whereas the contemporaneous intracontinental igneous rocks (e.g., those of the Songnen–Zhangguangcai Range Massif) consist of a bimodal igneous rock association (Yu et al., 2012; Xu et al., 2013). The former is consistent with an active continental margin setting (Gill, 1981), whereas the latter indicates an extensional environment (Yu et al., 2012). The polar variations in K_2O contents of the continental margin to intracontinental Early Jurassic igneous rocks are indicative of the initial subduction of the Paleo-Pacific Plate beneath Eurasia (Xu et al., 2013; Tang et al., 2018). Secondly, the widespread occurrence of Early Jurassic accretionary complexes in the eastern Asian continental margin (including northeastern China, Japan, and the Russian Far East) also indicates subduction of the Paleo-Pacific Plate beneath Eurasia (Wu et al., 2007a; Zhou et al., 2009; Fukuyama et al., 2013; Safonova and Santosh, 2014). Taken together, we conclude that uplift of the northeastern NCC was related to the onset of subduction of the Paleo-Pacific Plate beneath Eurasia in the Early Jurassic (Wang et al., 2016).

In summary, Early Triassic deposition in the northeastern NCC was controlled by the southward subduction of the Paleo-Asian oceanic plate, as well as by subduction and collision between the NCC and the YC (Fig. 13a). The absence of Middle Triassic strata in the northeastern NCC indicates the final closure of the Paleo-Asian Ocean during this time, which is also supported by the provenance of the Late Triassic deposits. The presence of XMOB material in Late Triassic deposits suggests that the Paleo-Asian Ocean had closed by this time. Rapid exhumation of the Su–Lu Orogenic Belt may have

resulted in the formation of a paleogeographic highland within the southeastern margin of the NCC (Fig. 13b). A sudden change in provenance was triggered by the rapid uplift of the XMOB in the Early Jurassic and was likely related to the onset of subduction of the Paleo-Pacific Plate beneath Eurasia at this time (Fig. 13c).

6 Conclusions

Based on the U–Pb ages of detrital and magmatic zircons, detrital zircon Hf isotopic systematics, and biostratigraphic records from early Mesozoic strata of the northeastern NCC, we draw the following conclusions.

(1) The early Mesozoic stratigraphic sequence of the northeastern NCC comprises, from bottom to top, the Early Triassic Heisonggou Formation (252–246 Ma), Late Triassic Changbai Formation (~227 Ma), Late Triassic Xiaoyingzi Formation, and Early Jurassic Yihe Formation.

(2) The Early Triassic Heisonggou Formation was sourced from the NCC, with ~42 % of sediment being derived from an area to the north of the basin and ~58 % from the area surrounding the basin. Approximately 88 % of sediments of the Late Triassic Xiaoyingzi Fm were sourced from the NCC, whereas the remaining ~12 % were derived from the XMOB. In contrast, >88 % of sediments of the Early Jurassic Yihe Fm were sourced from the XMOB, with only ~12 % being sourced from the NCC.

(3) Early Triassic deposition was controlled by both the southward subduction of the Paleo-Asian oceanic plate beneath the NCC and the northward subduction and collision between the NCC and YC. The Late Triassic deposition was possibly related to final closure of the Paleo-Asian Ocean and rapid exhumation of the Su–Lu Orogenic Belt between the NCC and YC. The sudden change in provenance recorded by Early Jurassic sediments, together with the coeval calc-alkaline volcanism and accretionary complex, indicates the rapid uplift of the XMOB and the onset of subduction of the Paleo-Pacific Plate beneath Eurasia in the Early Jurassic.

(4) Final closure of the Paleo-Asian Ocean likely occurred in the Middle Triassic, which is consistent with the lack of Middle Triassic strata in the northeastern NCC and the occurrence of Middle Triassic syn-collisional granitoids along the Changchun–Yanji Suture Belt.

Data availability. Original data underlying the material presented are available by contacting the authors.

Supplements. Supplementary Information; Table S1; Table S2.

Author contributions. Yi Ni Wang designed the study and wrote the main content. Wen Liang Xu designed the overall project and wrote the title. Feng Wang participated in fieldwork and data analysis. Xiao Bo Li modified and proofed the figures and captions.

Competing interests. The authors declare that they have no conflicts of interest.

Acknowledgements. We appreciate the journal editor and anonymous reviewers for their constructive and valuable comments. We would like to thank the staff of the State Key Laboratory of Geological Processes and Mineral Resources, China University of Geosciences, Wuhan, China, for helping with LA–ICP–MS zircon U–Pb dating and zircon Hf isotope analyses.

We thank Prof. Fu-Hong Gao identifying sedimentary rocks. This study was financially supported by the National Natural Science Foundation of China (Grants 41330206 and 41702030). Supporting data are included in the supporting information.

References

Andersen, T.: Correction of common lead in U–Pb analyses that do not report ^{204}Pb, Chem. Geol., 192, 59–79, https://doi.org/10.1016/S0009-2541(02)00195-X, 2002.

Beijing Bureau of Geology and Mineral Resources (BBGMR): Regional Geology of Beijing City, Geological Publishing House, Beijing, 1991 (in Chinese).

Bi, J. H., Ge, W. C., Yang, H., Wang, Z. H., Xu, W. L., Yang, J. H., Xing, D. H., and Chen, H. J.: Geochronology and geochemistry of Late Carboniferous–Middle Permian I-and A-type granites and gabbro-diorites in the eastern Jiamusi Massif, NE China: implications for petrogenesis and tectonic setting, Lithos, 266–267, 213–232, https://doi.org/10.1016/j.lithos.2016.10.001, 2016.

Cao, H. H., Xu, W. L., Pei, F. P., Wang, Z. W., Wang, F., and Wang, Z. J.: Zircon U–Pb geochronology and petrogenesis of the Late Paleozoic–Early Mesozoic intrusive rocks in the eastern segment of the northern margin of the North China Block, Lithos, 170–171, 191–207, https://doi.org/10.1016/j.lithos.2013.03.006, 2013.

Cao, H. H., Xu, W. L., Pei, F. P., Guo, P. Y., and Wang, F.: Permian tectonic evolution of the eastern section of the northern margin of the North China Plate: constraints from zircon U–Pb geochronology and geochemistry of the volcanic rocks, Acta Petrol. Sin., 28, 2733-2750, 2012 (in Chinese).

Corfu, F., Hanchar, J. M., Hoskin, P. W. O., and Kinny, P.: Atlas of zircon textures, Rev. Mineral. Geochem., 53, 469–500, https://doi.org/10.2113/0530469, 2003.

Cui, S. Q., Li, J. R., Wu, Z. H., Yi, M. C., Shen, S. M., Yin, H. R., and Ma, Y. S. (Eds.): Mesozoic and Cenozoic intracontinental orogenesis of the Yanshan area, Geological Publishing House, Beijing, 2002 (in Chinese).

Davis, G. A., Zheng, Y., Wang, C., Darby, B. J., Zhang, C., and Gehrels, G.: Mesozoic tectonic evolution of the Yanshan fold and thrust belt, with emphasis on Hebei and Liaoning Province, northern China, Beijing Geology, 194, 171–197, http://dx.doi. org/ 10.1130/0-8137-1194-0.171, 2001.

Dickinson, W. R., and Gehrels, G. E.: Sediment delivery to the Cordilleran foreland basin: Insights from U–Pb ages of detrital zircons in upper Jurassic and Cretaceous strata of the Colorado Plateau, Am. J. Sci., 308, 1041–1082, 2008.

Dong, Y., Ge, W. C., Yang, H., Xu, W. L., Zhang, Y. L., Bi, J. H., and Liu, X. W.: Geochronology, geochemistry, and Hf

isotopes of Jurassic intermediate-acidic intrusions in the Xing'an Block, northeastern China: petrogenesis and implications for subduction of the Paleo-Pacific oceanic plate, J. Asian Earth Sci., 118, 11–31, https://doi.org/10.1016/j.jseaes.2016.01.006, 2016.

Dong, Y., Ge, W. C., Yang, H., Zhao, G. C., Wang, Q. H., Zhang, Y. L., and Su, L.: Geochronology and geochemistry of Early Cretaceous volcanic rocks from the Baiyingaolao Formation in the central great Xing'an Range, NE China, and its tectonic implications, Lithos, 205, 168–184, https://doi.org/10.1016/j.lithos.2014.07.004, 2014.

Editing Group for Jilin Stratigraphic Chart (EGJS): The regional stratigraphic chart in the northeastern China (Jilin Province), Geological Publishing House, Beijing, 1975 (in Chinese).

Ernst, W. G., Tsujimori, T., Zhang, R., and Liou, J. G.: Permo–Triassic collision, subduction-zone metamorphism, and tectonic exhumation along the east Asian continental margin, Annu. Rev. Earth Pl. Sc., 35, 73–110, http://dx.doi.org/10.1146/annurev.earth.35.031306.140146, 2007.

Fukuyama, M., Ogasawara, M., Horie, K., and Lee, D. C.: Genesis of jadeite–quartz rocks in the Yorii area of the Kanto mountains, Japan, J. Asian Earth Sci., 63, 206–217, https://doi.org/10.1016/j.jseaes.2012.10.031, 2013.

Gao, S., Rudnick, R. L., Yuan, H. L., Liu, X. M., Liu, Y. S., Xu, W. L., Liang, W. L., Ayers, J., Wang, X. C., and Wang, Q. H.: Recycling lower continental crust in the North China Craton, Nature, 432, 892–897, http://dx.doi.org/10.1038/nature03162, 2004.

Ge, W. C., Wu, F. Y., Zhou, C. Y., and Zhang, J. H.: Porphyry Cu–Mo deposits in the eastern Xing'an–Mongolia Orogenic Belt: mineralization ages and their geodynamic implications, Chinese. Sci. Bull., 52, 3416–3427, https://doi.org/10.1007/s11434-007-0466-8, 2007 (in Chinese).

Gill, J. B.: Orogenic Andesites and Plate Tectonics, Springer, New York, 1981.

Guo, F.: Geological records of the Pacific Plate subduction in the northeast Asian continental magin: an overview, Bull. Mineral. Petrol. Geochem., 35, 1082–1092, http://dx.doi.org/10.3969/j.issn.1007-2082.2016. 06.002, 2016.

Hebei Bureau of Geology and Mineral Resources (JBGMR): Regional Geology of Hebei Province, Geological Publishing House, Beijing, 1989 (in Chinese).

Hu, Z. C., Gao, S., Liu, Y. S., Hu, S. H., Chen, H. H., and Yuan, H. L.: Signal enhancement in laser ablation ICP–MS by addition of nitrogen in the central channel gas, J. Anal. Atom. Spectrom., 23, 1093–1101, http://dx.doi.org/10. 1039/B804760J, 2008a.

Hu, Z. C., Liu, Y. S., Gao, S., Hu, S. H., Dietiker, R., and Günther, D.: A local aerosol extraction strategy for the determination of the aerosol composition in laser ablation inductively coupled plasma mass spectrometry, J. Anal. Atom. Spectrom., 23, 1192–1203, https://doi.org/10.1039/b803934h, 2008b.

Hu, Z. C., Liu, Y. S., Gao, S., Liu, W. G., Zhang, W., Tong, X. R., Lin, L., Zong, K. Q., Li, M., Chen, H.H., Zhou, L., and Yang, L.: Improved in situ Hf isotope ratio analysis of zircon using newly designed X skimmer cone and jet sample cone in combination with the addition of nitrogen by laser ablation multiple collector ICP–MS, J. Anal. Atom. Spectrom., 27, 1391–1399, http://doi.org/10.1039/c2ja30078h, 2012.

Inner Mongolia Bureau of Geology and Mineral Resources (IMBGMR): Regional Geology of Inner Mongolia Province, Geological Publishing House, Beijing, 1991 (in Chinese).

Jahn, B., Capdevila, R., Liu, D., Vernon, A., and Badarch, G.: Sources of Phanerozoic granitoids in the transect Bayanhongor–Ulaan Baatar, Mongolia: geochemical and Nd isotopic evidence and implications for Phanerozoic crustal growth, J. Asian Earth Sci., 23, 629–653, https://doi.org/10.1016/S1367-9120(03)00125-1, 2004.

Jia, D., Hu, R., Yan, L., and Qiu, X.: Collision belt between the Khanka block and the North China block in the Yanbian region, northeast China, J. Asian Earth Sci., 23, 211–219, https://doi.org/10.1016/S1367-9120(03)00123-8, 2004.

Jilin Bureau of Geology and Mineral Resources (JBGMR): Report of 1:200,000 regional geological research of Manjiang and Changbai area, Jilin Bureau of Geology and Mineral Resources, Changchun, 1963 (in Chinese).

Jilin Bureau of Geology and Mineral Resources (JBGMR): Report of 1:200,000 regional geological research of Fusong area, Jilin Bureau of Geology and Mineral Resources, Changchun, 1971 (in Chinese).

Jilin Bureau of Geology and Mineral Resources (JBGMR): Report of 1:200,000 regional geological research of Hunjiang and Ji'an area, Jilin Bureau of Geology and Mineral Resources, Changchun, 1976 (in Chinese).

Jilin Bureau of Geology and Mineral Resources (JBGMR): Regional Geology of Jilin Province, Geological Publishing House, Beijing, 1988 (in Chinese).

Jilin Bureau of Geology and Mineral Resources (JBGMR): Stratigraphy of Jilin Province, China University of Geosciences Press, Wuhan, 1997 (in Chinese).

Jilin Bureau of Geology and Mineral Resources (JBGMR): Report of 1:250,000 regional geological research of Jingyu, Hunjiang, and Changbai area, Jilin Bureau of Geology and Mineral Resources, Changchun, 2007 (in Chinese).

Li, H. Y., and Huang, X. L.: Constraints on the paleogeographic evolution of the North China Craton during the Late

Triassic–Jurassic, J. Asian Earth Sci., 70–71, 308–320, https://doi.org/10.1016/j.jseaes.2013.03.028, 2013.

Li, H. Y., Xu, Y. G., Huang, X. L., He, B., Luo, Z. Y., and Yan, B.: Activation of northern margino f the North China Craton in late Paleozoic: evidence from U–Pb dating and Hf isotopics of detrial zircons from the upper Carboniferous Taiyuan Formation in the Ningwu–Jingle basin, Chinese Sci. Bull., 54, 677–686, https://doi.org/10.1007/s11434-008-0444-9, 2009a (in Chinese).

Li, J. Y.: Permian geodynamic setting of northeast China and adjacent regions: closure of the Paleo-Asian Ocean and subduction of the Paleo-Pacific Plate, J. Asian Earth Sci., 26, 207–224, https://doi.org/10.1016/j.jseaes.2005.09.001, 2006.

Li, J. Y., Gao, L. M., Sun, G. H., Li, Y. P., and Wang, Y. B.: Shuangjingzi Middle Triassic syn-collisional crust-derived granite in the east Inner Mongolia and its constraint on the timing of collision between Siberian and Sino-Korean paleo-plates, Acta Petrol. Sin., 23, 565–582, 2007 (in Chinese).

Li, J. Y., Niu, B. G., Song, B., Xu, W. X., Zhang, Y. H., and Zhao, Z. R. (Eds.): Crustal formation and evolution of northern Changbai Mountains, northeast China, Geological Publishing House, Beijing, 1999 (in Chinese).

Li, X. H., Liu, Y., Li, Q. L., Guo, C. H., and Chamberlain, K. R.: Precise determination of Phanerozoic zircon Pb/Pb age by multi-collector SIMS without external standardization, Geochem. Geophy. Geosy., 10(6), Q04010, http://dx.doi. org/ 10.1029/2009GC002400, 2009b.

Li, Z. H., Qu, H. J., and Gong, W. B.: Late Mesozoic basin development and tectonic setting of the northern North China Craton, J. Asian Earth Sci., 114, 115–139, https://doi.org/10.1016/j.jseaes.2015.05.029, 2015.

Liaoning Bureau of Geology and Mineral Resources (LBGMR): Regional Geology of Liaoning Province, Geological Publishing House, Beijing, 1989 (in Chinese).

Lin, Q., Ge, W. C., Sun, D. Y., Wu, F. Y., Chong, K. W., Kyung, D. M., Myung, S. J., Moon, W., Chi, S. K., and Sung, H. Y.: Tectonic significance of Mesozoic volcanic rocks in northeastern China, Sci. Geol. Sin., 33, 129 –139, 1998 (in Chinese).

Liu, F. L., Gerdes, A., and Xue, H. M.: Differential subduction and exhumation of crustal slices in the Sulu Hp–Uhp metamorphic terrane: insights from mineral inclusions, trace elements, U–Pb and Lu–Hf isotope analyses of zircon in orthogneiss, J. Metam. Geol., 27, 805–825, https://doi.org/10.1111/j.1525-1314.2009. 00833.x, 2009.

Liu, F. L., Gerdes, A., and Liu, P. H.: U–Pb, trace element and Lu–Hf properties of unique dissolution-reprecipitation zircon from Uhp eclogite in SW Sulu terrane, eastern China, Gondwana Res., 22, 169–183, https://doi.org/10.1016/j.gr.2011.11.007, 2012.

Liu, Y. Q., Kuang, H. W., Peng, N., Xu, H., Zhang, P., Wang, N. S., and An, W.: Mesozoic basins and associated Palaeogeographic evolution in North China, J. Palaeogeog., 4, 189–202, https://doi.org/10.3724/SP.J.1261.2015.00073, 2015.

Liu, Y. S., Hu, Z. C., Zong, K. Q., Gao, C. G., Gao, S., Xu, J., and Chen, H. H.: Reappraisement and refinement of zircon U–Pb isotope and trace element analyses by LA–ICP–MS, Chinese Sci. Bull., 55, 1535–1546, https://doi.org/10.1007/ s11434-010-3052-4, 2010.

Ludwig, K. R.: User's manual for Isoplot 3.00: A geochronological toolkit for Microsoft excel, special publication 4, Berkeley Geochronology Center, 2003.

Ma, X. Y, and Wu, Z. W.: Early tectonic evolution of China, Precambrian Res., 14, 185–202, https://doi.org/10.1016/0301-9268(81)90038-3, 1981.

Meng, E., Xu, W. L., Pei, F. P., Yang, D. B., Yu, Y., and Zhang, X. Z.: Detrital-zircon geochronology of Late Paleozoic sedimentary rocks in eastern Heilongjiang Province, NE China: implications for the tectonic evolution of the eastern segment of the Central Asian Orogenic Belt, Tectonophysics, 485, 42–51, https://doi.org/10.1016/j.tecto. 2009.11.015, 2010.

Meng, Q. R.: What drove late Mesozoic extension of the northern China–Mongolia tract? Tectonophysics, 369, 155–174, https://doi.org/10.1016/S0040-1951(03) 00195-1, 2003.

Meng, Q. R., Wei, H. H., Qu, Y. Q., and Ma, S. X.: Stratigraphic and sedimentary records of the rift to drift evolution of the northern North China Craton at the Paleo–to Mesoproterozoic transition, Gondwana Res., 20, 205–218, https://doi.org/ 10.1016/j.gr.2010.12.010, 2011.

Meng, Q. R., Wei, H. H., Wu, G. L., and Duan, L.: Early Mesozoic tectonic settings of the northern North China Craton, Tectonophysics, 611, 155–166, http://dx.doi. org/10.1016/j.tecto.2013.11.015, 2014.

Meng, Q. R.: Development of sedimentary basins in eastern China during the Yanshanian Period, Bull. Mineral. Petrol. Geochem., 36, 567–569, 2017 (in Chinese).

Meng, Q. R., Wu, G. L., Fan, L. G., and Wei, H. H.: Early Mesozoic evolution of sedimentary basins and tectonic settings of the North China Craton, Sci. China (Earth Sci.), under review, 2018.

Pei, F. P., Xu, W. L., Yang, D. B., Yu, Y., Meng, E., and Zhao, Q. G.: Petrogenesis of late Mesozoic granitoids in southern Jilin Province, northeastern China: geochronological, geochemical, and Sr–Nd–Pb isotopic evidence, Lithos, 125, 27–39. https://doi. org/ 10.1016/j.lithos.2011.01.004, 2011.

Pei, F. P., Zhang, Y., Wang, Z. W., Cao, H. H., Xu, W. L., Wang, Z. J., Wang, F. and Yang, C.: Early–Middle Paleozoic

subduction-collision history of the south-eastern central Asian orogenic belt: evidence from igneous and metasedimentary rocks of central Jilin Province, NE China, Lithos, 261, 164–180, https://doi.org/10.1016/j.lithos.2015.12.010, 2016.

Pei, F. P., Wang, Z. W., Cao, H. H., Xu, W. L., and Wang, F.: Petrogenesis of the Early Paleozoictonalite in the central Jilin Province: evidence from zircon U–Pb chronology and geochemistry, Acta Petrol. Sin., 30, 2009–2019, 2014 (in Chinese).

Pei, F. P., Xu, W. L., Yu, Y., Zhao, Q. G., and Yang, D. B.: Petrogenesis of the Late Triassic Mayihe Pluton in southern Jilin Province: evidence from zircon U–Pb geochronology and geochemistry, J. Jilin Univ. (Earth Sci. Edition), 38, 351–362, 2008 (in Chinese).

Sengör, A. M. C., and Natal'in, B. A.: Paleotectonics of Asia: Fragments of a synthesis, in: The Tectonic Evolution of Asia, Cambridge University Press, London, 486–640, 1996.

Shanxi Bureau of Geology and Mineral Resources (SBGMR): Regional Geology of Shanxi Province, Geological Publishing House, Beijing, 1989 (in Chinese).

Shen, S. Z., Zhang, H., Shang, Q. H., and Li, W. Z.: Permian stratigraphy and correlation of northeast China: a review, J. Asian Earth Sci., 26, 304–326, https://doi.org/10.1016/j.jseaes.2005.07.007, 2006.

Safonova, I. Y., and Santosh, M.: Accretionary complexes in the Asia-Pacific region: tracing archives of ocean plate stratigraphy and tracking mantle plumes, Gondwana Res., 25, 126–158, https://doi.org/10.1016/j.gr.2012.10.008, 2014.

Shi, G. R.: The marine Permian of east and northeast Asia: an overview of biostratigraphy, palaeobiogeography and palaeogeographical implications, J. Asian Earth Sci., 26, 175–206, https://doi.org/10.1016/j.jseaes.2005.11.004, 2006.

Si, X. J., and Zhou, Z. Y. (Eds.): Mesozoic continental strata in China, Science Press, Beijing, 1962 (in Chinese).

Sun, D. Y., Wu, F. Y., Zhang, Y. B., and Gao, S.: The final closing time of Xiramuron–Changchun–Yanji plate suture zone: evidence from the Dayushan granitic pluton of Jilin, J. Jilin Univ. (Earth Sci. Edition), 34, 174–181, 2004 (in Chinese).

Sun, M. D., Xu, Y. G., Wilde, S. A., Chen, H. L., and Yang, S. F.: The Permian Dongfanghong island-arc gabbro of the Wandashan Orogen, NE China: implications for Paleo-Pacific subduction, Tectonophysics, 659, 122–136, https://doi.org/10.1016/ j.tecto. 2015.07.034, 2015.

Tang, J., Xu, W. L., Wang, F., and Ge, W. C.: Subduction history of the Paleo-Pacific slab beneath Eurasian continent: Mesozoic–Paleogene magmatic records in northeast Asia, Sci. China (Earth Sci.), 61, 527–559, https://doi.org/10.1007/s11430-017-9174-1, 2018.

Tang, J., Xu, W. L., Wang, F., Wang, W., Xu, M. J., and Zhang, Y. H.: Geochronology and geochemistry of Neoproterozoic

magmatism in the Erguna Massif, NE China: Petrogenesis and implications for the breakup of the Rodinia supercontinent, Precambrian Res., 224, 597–611, https://doi.org/10.1016/j.precamres.2012.10.019, 2013.

Tang, J., Xu., W. L., and Wang, F.: Rock associations and their spatial-temporal variations of the early Mesozoic igneous rocks in the NE Asia: constraints on the initial subduction timing of the Paleo-Pacific Plate, Bull. Mineral. Petrol. Geochem., 35, 1181–1194, https://doi.org/10.3969/ j.issn.l007-2802.2016.06.009, 2016 (in Chinese).

Wang, F., Xu, W. L., Gao, F. H., Zhang, H. H., Pei, F. P., Zhao, L., and Yang, Y.: Precambrian terrane within the Songnen–Zhangguangcai Range Massif, NE China: evidence from U–Pb ages of detrital zircons from the Dongfengshan and Tadong groups, Gondwana Res., 26, 402–413, https://doi.org/10.1016/j.gr.2013.06.017, 2014.

Wang, F., Xu, W. L., Meng, E., Cao, H. H., and Gao, F. H.: Early Paleozoic amalgamation of the Songnen–Zhangguangcai Range and Jiamusi Massifs in the eastern segment of the central Asian orogenic belt: geochronological and geochemical evidence from granitoids and rhyolites, J. Asian Earth Sci., 49, 234–248, https://doi.org/10.1016/j.jseaes.2011.09.022, 2012.

Wang, F., Xu, W. L., Xu, Y. G., Gao, F. H., and Ge, W. C.: Late Triassic bimodal igneous rocks in eastern Heilongjiang Province, NE China: implications for the initiation of subduction of the Paleo-Pacific Plate beneath Eurasia, J. Asian Earth Sci., 97, 406–423. https://doi.org/10.1016/j.jseaes.2014.05.025, 2015a.

Wang, F., Xu, Y. G., Xu, W. L., Yang, L., and Wu, Wei.: Early Jurassic calc-alkaline magmatism in northeast China: Magmatic response to subduction of the Paleo-Pacific Plate beneath the Eurasian continent, J. Asian Earth Sci., 143, 249–268. http://dx.doi.org/10.1016/j.jseaes.2017.04.018, 2017.

Wang, Z. J., Xu, W. L., Pei, F. P., Wang, Z. W., Li, Y., and Cao, H. H.: Geochronology and geochemistry of Middle Permian–Middle Triassic intrusive rocks from central–eastern Jilin Province, NE China: constraints on the tectonic evolution of the eastern segment of the Paleo-Asian ocean, Lithos, 238, 13–25, https://doi.org/10.1016/ j.lithos.2015.09.019, 2015b.

Wang, Z. W., Pei, F. P., Xu, W. L., Cao, H. H., Wang, Z. J., and Zhang, Y.: Tectonic evolution of the eastern central Asian orogenic belt: evidence from zircon U–Pb–Hf isotopes and geochemistry of early Paleozoic rocks in Yanbian region, NE China, Gondwana Res., 38, 334–350, https://doi.org/10.1016/j.gr.2016.01.004, 2016.

Wilde, S. A., and Zhou, J. B.: The late Paleozoic to Mesozoic evolution of the eastern margin of the central Asian orogenic belt in China, J. Asian Earth Sci., 113, 909–921, https://doi.org/10.1016/j.jseaes.2015.05.005, 2015.

Wu, F. Y., Jahn, B. M., Wilde, S., and Sun, D. Y.: Phanerozoic continental crustal growth: Sr–Nd isotopic evidence from the granitesin northeastern China, Tectonophysics, 328, 87–113, 2000.

Wu, F. Y., Sun, D. Y., Ge, W. C., Zhang, Y. B., Grant, M. L., Wilde, S. A., and Jahn, B. M.: Geochronology of the

Phanerozoic granitoids in northeastern China, J. Asian Earth Sci., 41, 1–30, https://doi.org/10.1016/j.jseaes.2010.11.014, 2011.

Wu, F. Y., Sun, D. Y., Jahn, B. M., and Wilde, S.: A Jurassic garnet-bearing granitic pluton from NE China showing tetrad REE patterns, J. Asian Earth Sci., 23, 731–744, https://doi.org/10.1016/S1367-9120(03)00149-4, 2004.

Wu, F. Y., Sun, D. Y., Li, H., Jahn, B. M., and Wilde, S.: A-type granites in northeastern China: age and geochemical constraints on their petrogenesis, Chem. Geol., 187, 143–173, https://doi.org/10.1016/S0009-2541(02)00018-9, 2002.

Wu, F. Y., Yang, J. H., Lo, C. H., Wilde, S. A., Sun, D. Y., and Jahn, B. M.: The Heilongjiang group: a Jurassic accretionary complex in the Jiamusi Massif at the western pacific margin of northeastern China, Island Arc, 16, 156–172, https://doi.org/10.1111/j.1440-1738.2007.00564.x, 2007a.

Wu, F. Y., Zhao, G. C., Sun, D. Y., Wilde, S. A., and Yang, J. H.: The Hulan Group: its role in the evolution of the Central Asian Orogenic Belt of NE China, J. Asian Earth Sci., 30, 542–556, https://doi.org/10.1016/j.jseaes.2007.01.003, 2007b.

Xu, B., Zhao, P., Bao, Q. Z., Zhou, Y. H., Wang, Y. Y., and Luo, Z. W.: Preliminary study on the pre-Mesozoic tectonic unit division of the Xing–Meng Orogenic Belt (XMOB), Acta Petrol. Sin., 30, 1841–1857, 2014 (in Chinese).

Xu, B., Zhao, P., Wang, Y. Y., Liao, W., Luo, Z. W., Bao, Q. Z., and Zhou, Y. H.: The pre–Devonian tectonic framework of Xing'an–Mongolia Orogenic Belt (XMOB) in North China, J. Asian Earth Sci., 97, 183–196, https://doi.org/10.1016/j.jseaes.2014.07.020, 2015.

Xu, H., Liu, Y. Q., Kuang, H. W, and Peng, N.: Sedimentary response to the intracontinental orogenic process: insight from the anatomy of a small Mesozoic basin in western Yanshan, northern North China, Int. Geol. Rev., 58, 1528–1556, https://doi.org/10.1080/00206814.2016.1168323, 2016.

Xu, W. L., Ji, W. Q., Pei, F. P., Meng, E., Yu, Y., Yang, D. B., and Zhang, X. Z.: Triassic volcanism in eastern Heilongjiang and Jilin provinces, NE China: chronology, geochemistry, and tectonic implications, J. Asian Earth Sci., 34, 392–402, https://doi.org/10.1016/j.jseaes.2008.07.001, 2009.

Xu, W. L., Pei, F. P., Wang, F., Meng, E., Ji, W. Q., Yang, D. B., and Wang, W.: Spatial-temporal relationships of Mesozoic volcanic rocks in NE China: constraints on tectonic overprinting and transformations between multiple tectonic systems, J. Asian Earth Sci., 74, 167–193, https://doi.org/10.1016/j.jseaes.2013.04.003, 2013.

Xu, W. L., Wang, F., Meng, E., Gao, F. H., Pei, F. P., and Yu, J. J.: Paleozoic–early Mesozoic tectonic evolution in the eastern Heilongjiang Province, NE China: evidence from igneous rock association and U–Pb geochronology of detrital zircons, J. Jilin Univ. (Earth Sci. Edition), 42, 1378–1389, https://doi.org/10.13278/j.cnki.jjuese.2012.05.024, 2012 (in

Chinese).

Yang, D. B., Yang, H. T., Shi, J. P., Xu, W. L., and Wang, F.: Sedimentary response to the paleogeographic and tectonic evolution of the southern North China Craton during the late Paleozoic and Mesozoic, Gondwana Res., 49, https://doi.org/10.1016/j.gr.2017.06.009, 2017.

Yang, H., Ge, W. C., Yu, Q., Ji, Z., Liu, X. W., Zhang, Y. L., Tian, D. X.: Zircon U–Pb–Hf isotopes, bulk-rock geochemistry and petrogenesis of Middle to Late Triassic I-type granitoids in the Xing'an Block, northeast China: implications for early Mesozoic tectonic evolution of the central great Xing'an range, J. Asian Earth Sci., 119, 30–48, https://doi.org/10.1016/j.jseaes.2016.01.012, 2016.

Yang, H., Ge, W. C., Zhao, G. C., Dong, Y., Xu, W. L., Ji, Z., and Yu, J. J.: Late Triassic intrusive complex in the Jidong region, Jiamusi–Khanka Block, NE China: geochemistry, zircon U–Pb ages, Lu–Hf isotopes, and implications for magma mingling and mixing, Lithos, 224–225, 143–159, https://doi.org/10.1016/j.lithos.2015.03.001, 2015a.

Yang, H., Ge, W. C., Zhao, G. C., Yu, J. J., and Zhang, Y. L.: Early Permian–Late Triassic granitic magmatism in the Jiamusi–Khanka Massif, eastern segment of the Central Asian Orogenic Belt and its implications, Gondwana Res., 27, 1509–1533, https://doi.org/10.1016/j.gr.2014.01.011, 2015b.

Yang, J. H., Wu, F. Y., Shao, J. A., Wilde, S. A., Xie, L. W., and Liu, X. M.: Constraints on the timing of uplift of the Yanshan Fold and Thrust Belt, north China, Earth Planet. Sci. Lett., 246, 336–352, https://doi.org/10.1016/j.epsl.2006.04.029, 2006.

Yang, J. H., Wu, F. Y., Wilde, S. A., and Liu, X. M.: Petrogenesis of Late Triassic granitoids and their enclaves with implications for post-collisional lithospheric thinning of the Liaodong peninsula, North China Craton, Chem. Geol., 242, 155–175, https://doi.org/10.1016/j.chemgeo.2007.03.007, 2007.

Yu, J. J., Wang, F., Xu, W. L., Gao, F. H., and Pei, F. P.: Early Jurassic mafic magmatism in the lesser Xing'an–Zhangguangcai Range, NE China, and its tectonic implications: constraints from zircon U–Pb chronology and geochemistry, Lithos, 142–143, 256–266, https://doi.org/10.1016/j.lithos.2012.03.016, 2012.

Yu, Y., Xu, W. L., Pei, F. P., Yang, D. B., and Zhao, Q. G.: Chronology and geochemistry of Mesozoic volcanic rocks in the Linjiang area, Jilin Province and their tectonic implications, Acta Geol. Sin.(English Edition), 83, 245–257, https://doi.org/10.1111/j.1755-6724.2009.00039.x, 2009.

Yuan, H. L., Gao, S., Liu, X. M., Li, H. M., Günther, D., and Wu, F. Y.: Accurate U–Pb age and trace element determinations of zircon by laser ablation inductively coupled plasmamass spectrometry, Geost. Newslett, 28, 353–370, 2004.

Zhang, S. H., Zhao, Y., Davis, G. A., Ye, H., and Wu, F.: Temporal and spatial variations of Mesozoic magmatism and deformation in the North China Craton: implications for lithospheric thinning and decratonization, Earth Sci. Rev., 131, 49–87, https://doi.org/10.1016/j.earscirev.2013.12.004, 2014.

Zhang, S. H., Zhao, Y., Kröner, A., Liu, X. M., Xie, L. W., and Chen, F. K.: Early Permian plutons from the northern North China block: constraints on continental arc evolution and convergent margin magmatism related to the Central Asian Orogenic Belt, Int. J. Earth Sci., 98, 1441–1467, https://doi.org/10.1007/s00531-008-0368-2, 2009.

Zhang, S. H., Zhao, Y., Liu, J. M., Hu, J. M., Song, B., Liu, J., and Wu, H.: Geochronology, geochemistry and tectonic setting of the late Paleozoic–early Mesozoic magmatism in the northern margin of the North China Block: A preliminary review, Acta Petrol. Mineral., 29, 824–842, https://doi.org/10.3969/j.issn.1000-6524.2010.06.017, 2010 (in Chinese).

Zhang, Y. B., Wu, F. Y., Wilde, S. A., Zhai, M. G., Lu, X. P., and Sun, D. Y.: Zircon U–Pb ages and tectonic implications of 'early Paleozoic' granitoids at Yanbian, Jilin province, NE China, Island Arc, 13, 484–505, https://doi.org/10.1111/j.1440-1738. 2004.00442.x, 2004.

Zhao, G. C, Wilde, S. A., Cawood, P. A., and Sun, M.: Archean blocks and their boundaries in the North China Craton: lithological, geochemical, structural and P–T, path constraints and tectonic evolution, Precambrian Res., 107, 45–73, https://doi.org/ 10.1016/S0301-9268(00)00154-6, 2001.

Zhao, L. L., and Zhang, X. Z.: Petrological and geochronological evidences of tectonic exhumation of Heilongjiang complex in the eastern part of Heilongjiang Province, China, Acta Petrol. Sin., 27, 1227–1234, 2011 (in Chinese).

Zhao, P., Jahn, B. M., and Xu, B.: Elemental and Sr–Nd isotopic geochemistry of Cretaceous to early Paleogene granites and volcanic rocks in the Sikhote–Alin Orogenic Belt (Russian Far East) and their implication on regional tectonic evolution, J. Asian Earth Sci., https://doi.org/10.1016/j.jseaes.2017.06.017, 2017.

Zheng, Y. F., Fu, B., Gong, B., and Li, L.: Stable isotope geochemistry of ultrahigh pressure metamorphic rocks from the Dabie–Sulu orogen in China: implications for geodynamics and fluid regime, Earth Sci. Rev., 62, 105–161, 2003.

Zheng, Y. F., Xiao, W. J., and Zhao, G. C.: Introduction to tectonics of China, Gondwana Res., 23, 1189–1206, https://doi.org/10.1016/j.gr.2012.10.001, 2013.

Zhou, J. B., and Li, L.: The Mesozoic accretionary complex in northeast China: evidence for the accretion history of Paleo-Pacific subduction, J. Asian Earth Sci., 145, 91–100, https://doi.org/10.1016/j.jseaes.2017.04.013, 2017.

Zhou, J. B., Cao, J. L., Wilde, S. A., Zhao, G. C., Zhang, J. J., and Wang, B.: Paleo-Pacific subduction-accretion: evidence from geochemical and U–Pb zircon dating of the Nadanhada accretionary complex, NE China, Tectonics, 33, 2444–2466,

https://doi.org/10.1002/2014TC003637, 2015.

Zhou, J. B., Wilde, S. A., Zhang, X. Z., Zhao, G. C., Zheng, C. Q., Wang, Y. J., and Zhang, X. H.: The onset of Pacific margin accretion in NE China: evidence from the Heilongjiang high-pressure metamorphic belt, Tectonophysics, 478, 230–246, https://doi.org/10.1016/j.tecto.2009.08.009, 2009.

Zhou, J. B., Wilde, S. A., Zhao, G. C., Zhang, X. Z., Zheng, C. Q., and Wang, H.: New Shrimp U–Pb zircon ages from the Heilongjiang High-Pressure Belt: constraints on the Mesozoic evolution of NE China, Am. J. Sci., 310, 1024–1053, https://doi.org/10.2475/09.2010.10, 2010.

Zhu, G. X.: The discovery of the assemblage of bivalve fossils in the Late Triassic fresh water in the Xiaoyingzi Formation, Fusong, Jilin province, Jilin Geology, 1, 13–21, 1991(in Chinese).

Figure captions

Figure 1: Geological sketch map of the northeastern North China Craton. JJOB: Jing–Ji Orogenic Belt.

Figure 2: Geological map of the Linjiang area showing early Mesozoic strata and the three study sections.

Figure 3: Early Mesozoic stratigraphy of the northeastern NCC, sampling sites, and dating results. The ages refer to the youngest age populations of samples.

Figure 4: Stratotype outcrop of the Heisonggou Formation and sampling locations. The location of the stratotype is indicated by the dotted line in Fig. 2 (section 3). The numbers in circles show the sequence of beds in the section. The ages refer to the youngest zircon age populations of samples.

Figure 5: Stratotype outcrop of the Xiaoyingzi Formation and sampling locations. The location of the stratotype is indicated by the dotted line in Fig. 2 (section 1). The numbers in circles indicate the sequence of beds in the section. The ages refer to the youngest zircon age populations of samples. The dotted line represents vegetation cover.

Figure 6: Stratotype outcrop of the Yihe Formation and sampling locations. The location of the stratotype is indicated by the dotted line in Fig. 2 (section 2). The numbers in circles indicate the sequence of beds in the section. The ages refer to the youngest zircon age populations of samples.

Figure 7: Photomicrographs of representative early Mesozoic samples (cross-polarized light). (a) Sample 16LJ6-1, a medium-grained feldspathic quartz sandstone of the Heisonggou Fm; (b) Sample 15LJ4-11, a fine-grained feldspathic quartz sandstone of the Heisonggou Fm; (c) Sample 15LJ4-6, an andesite that intrudes the Heisonggou Fm; (d) Sample 15JFS1-1, a medium-grained feldspathic quartz sandstone of the Xiaoyingzi Fm; (e) Sample 15JFS2-1, a diabase porphyrite that intrudes the Xiaoyingzi Fm; (f) Sample 15JFS10-1, a pyroxene andesite of the Guosong Fm; (g) Sample 16LJ1-1, an andesite of the

Changbai Fm; (h) Sample 16LJ3-1, a tuffaceous siltstone of the Yihe Fm. Af: alkali-feldspar; Pl: plagioclase; Px: pyroxene; Q: quartz.

Figure 8: Cathodoluminescence (CL) images of selected zircon grains from early Mesozoic strata. White circles indicate the locations of U–Pb dating analyses and blue circles show the locations of *in situ* Hf analyses. Values under and above the images indicate zircon U–Pb ages and measured $\varepsilon_{Hf}(t)$ values, respectively.

Figure 9: U–Pb concordia diagram for zircon grains from the sedimentary and igneous rocks within early Mesozoic strata.

Figure 10: Hf isotopic compositions of detrital zircon grains from early Mesozoic strata of the northeastern NCC. XMOB: Xing'an–Mongolia Orogenic Belt; YFTB: Yanshan Fold and Thrust Belt (Yang et al., 2006).

Figure 11: Correlation between the early Mesozoic stratigraphy of the northern and northeastern NCC (the stratigraphic sequence of the northern NCC is from Meng et al., 2018).

Figure 12: Relative probability diagram of detrital zircon grain ages from early Mesozoic strata of the northeastern NCC.

Figure 13: Paleotectonic evolution of northeastern China in the early Mesozoic, showing the paleogeographic evolution and provenance of early Mesozoic basins. (a) Early Triassic: southward subduction of the Paleo-Asian oceanic plate and subduction and collision between the NCC and YC; (b) Late Triassic: final closure of the Paleo-Asian Ocean and post-collisional exhumation of the Su–Lu Orogenic Belt; (c) Early Jurassic: rapid uplift of the XMOB and the onset of subduction of the Paleo-Pacific Plate beneath Eurasia.

Figure 1

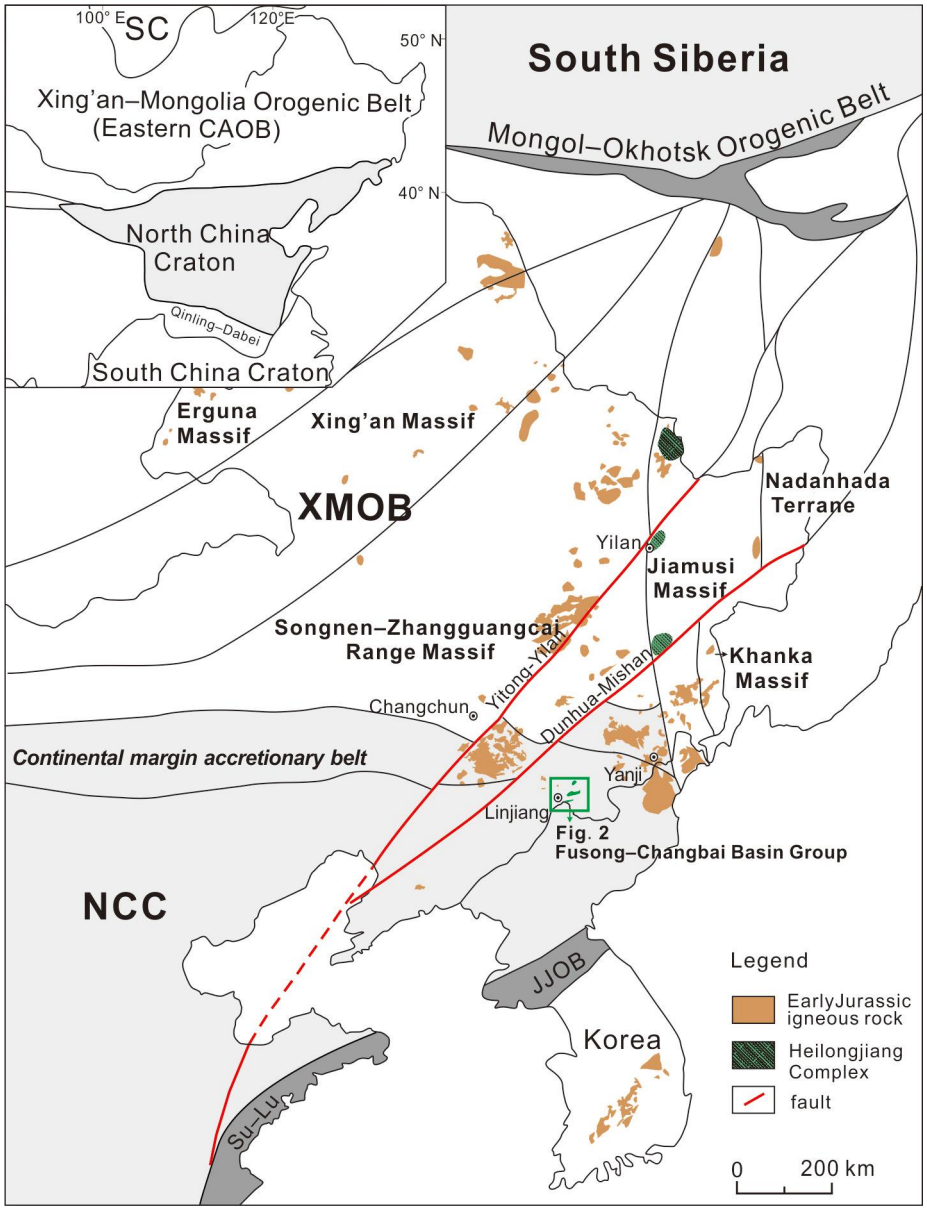
100° E
SC
120°E
50° N
40° N
South Siberia
Xing'an–Mongolia Orogenic Belt
(Eastern CAOB)
Mongol–Okhotsk Orogenic Belt
North China
Craton
Qinling–Dabei
South China Craton
Erguna
Massif
Xing'an Massif
XMOB
Nadanhada
Terrane
Yilan
Jiamusi
Massif
Songnen–Zhangguangcai
Range Massif
Yitong-Yilan
Dunhua-Mishan
Khanka
Massif
Changchun
Continental margin accretionary belt
Yanji
Linjiang
Fig. 2
Fusong–Changbai Basin Group
NCC
JJOB
Korea
Su-Lu
Legend
EarlyJurassic
igneous rock
Heilongjiang
Complex
fault
0
200 km

5

Figure 2

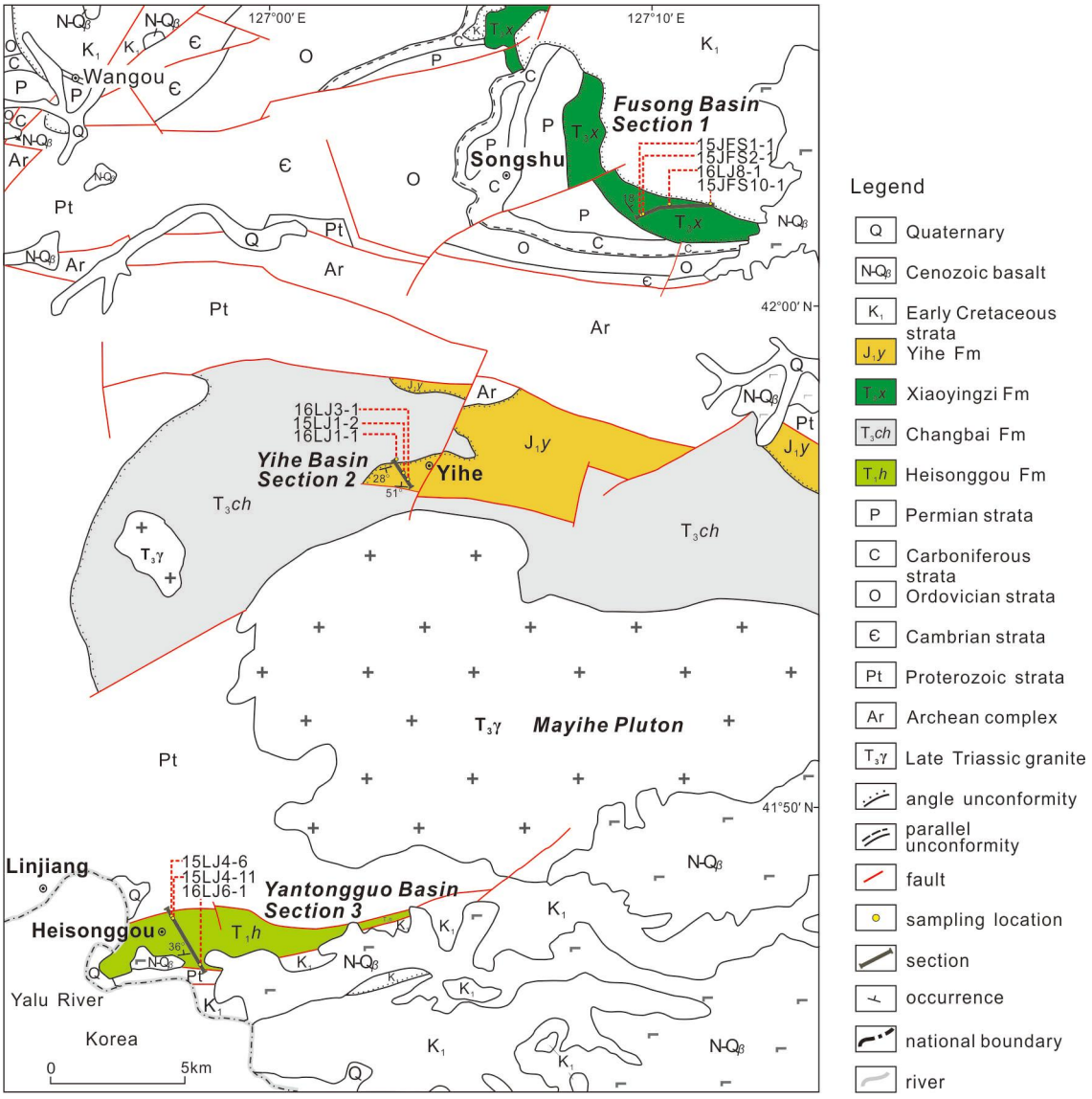
127°00′ E
127°10′ E
42°00′ N
41°50′ N
Wangou
Songshu
Fusong Basin
Section 1
15JFS1-1
15JFS2-1
16LJ8-1
15JFS10-1
Yihe Basin
Section 2
16LJ3-1
15LJ1-2
16LJ1-1
Yihe
28°
51°
Mayihe Pluton
Linjiang
Heisonggou
Yantongguo Basin
Section 3
15LJ4-6
15LJ4-11
16LJ6-1
36°
Yalu River
Korea
0
5km
Legend
Quaternary
Cenozoic basalt
Early Cretaceous strata
Yihe Fm
Xiaoyingzi Fm
Changbai Fm
Heisonggou Fm
Permian strata
Carboniferous strata
Ordovician strata
Cambrian strata
Proterozoic strata
Archean complex
Late Triassic granite
angle unconformity
parallel unconformity
fault
sampling location
section
occurrence
national boundary
river

5

Figure 3

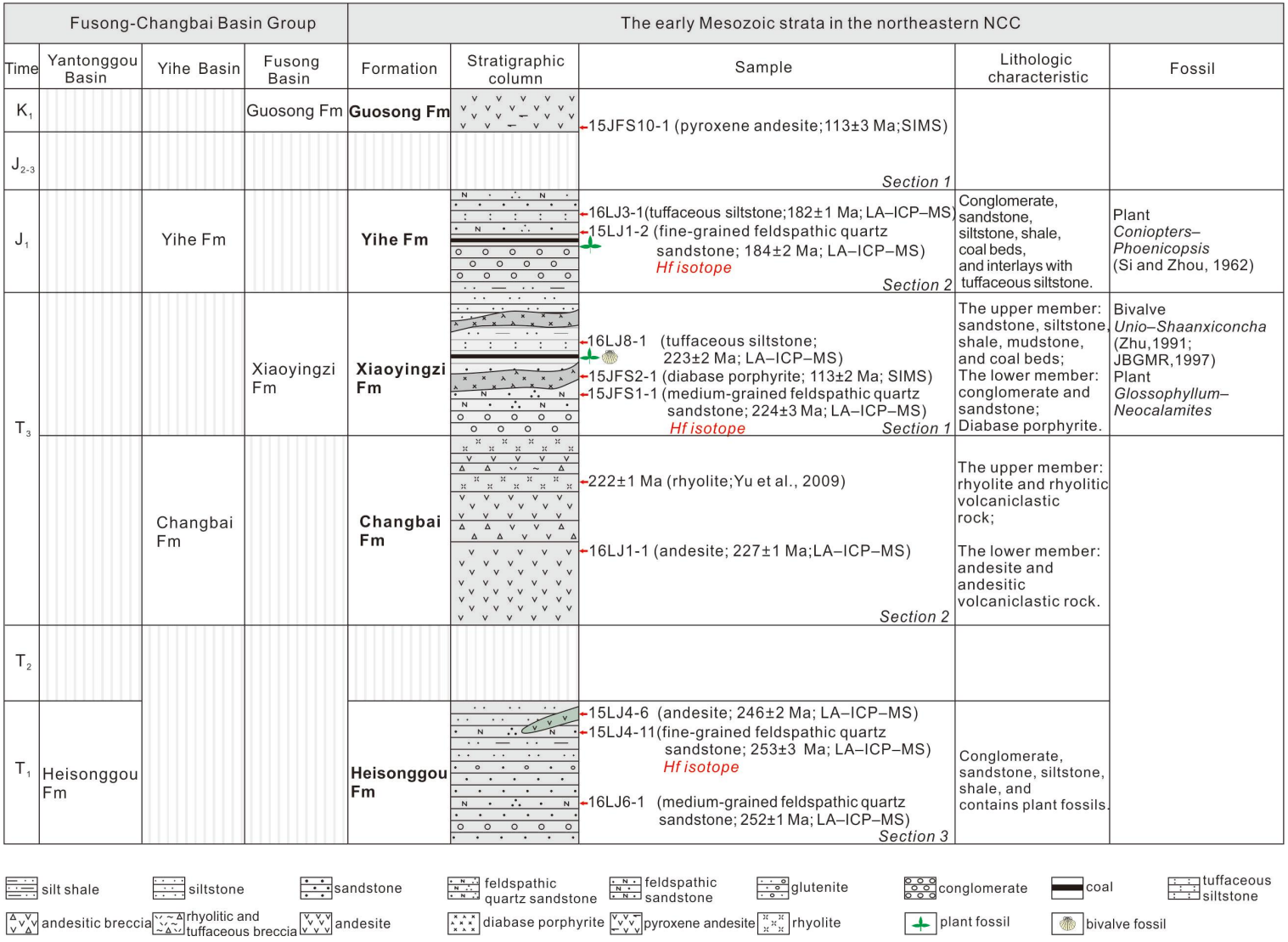
Fusong-Changbai Basin Group
The early Mesozoic strata in the northeastern NCC
Time
Yantonggou Basin
Yihe Basin
Fusong Basin
Formation
Stratigraphic column
Sample
Lithologic characteristic
Fossil
K1
Guosong Fm
Guosong Fm
15JFS10-1 (pyroxene andesite;113±3 Ma;SIMS)
Section 1
J2-3
J1
Yihe Fm
Yihe Fm
16LJ3-1(tuffaceous siltstone;182±1 Ma; LA–ICP–MS)
15LJ1-2 (fine-grained feldspathic quartz sandstone; 184±2 Ma; LA–ICP–MS)
Hf isotope
Section 2
Conglomerate, sandstone, siltstone, shale, coal beds, and interlays with tuffaceous siltstone.
Plant
Coniopters–Phoenicopsis
(Si and Zhou, 1962)
T3
Xiaoyingzi Fm
Xiaoyingzi Fm
16LJ8-1 (tuffaceous siltstone; 223±2 Ma; LA–ICP–MS)
15JFS2-1 (diabase porphyrite; 113±2 Ma; SIMS)
15JFS1-1 (medium-grained feldspathic quartz sandstone; 224±3 Ma; LA–ICP–MS)
Hf isotope
Section 1
The upper member: sandstone, siltstone, shale, mudstone, and coal beds;
The lower member: conglomerate and sandstone;
Diabase porphyrite.
Bivalve
Unio–Shaanxiconcha
(Zhu,1991; JBGMR,1997)
Plant
Glossophyllum–Neocalamites
Changbai Fm
Changbai Fm
222±1 Ma (rhyolite;Yu et al., 2009)
16LJ1-1 (andesite; 227±1 Ma;LA–ICP–MS)
Section 2
The upper member: rhyolite and rhyolitic volcaniclastic rock;
The lower member: andesite and andesitic volcaniclastic rock.
T2
T1
Heisonggou Fm
Heisonggou Fm
15LJ4-6 (andesite; 246±2 Ma; LA–ICP–MS)
15LJ4-11(fine-grained feldspathic quartz sandstone; 253±3 Ma; LA–ICP–MS)
Hf isotope
16LJ6-1 (medium-grained feldspathic quartz sandstone; 252±1 Ma; LA–ICP–MS)
Section 3
Conglomerate, sandstone, siltstone, shale, and contains plant fossils.
silt shale
siltstone
sandstone
feldspathic quartz sandstone
feldspathic sandstone
glutenite
conglomerate
coal
tuffaceous siltstone
andesitic breccia
rhyolitic and tuffaceous breccia
andesite
diabase porphyrite
pyroxene andesite
rhyolite
plant fossil
bivalve fossil

Figure 4

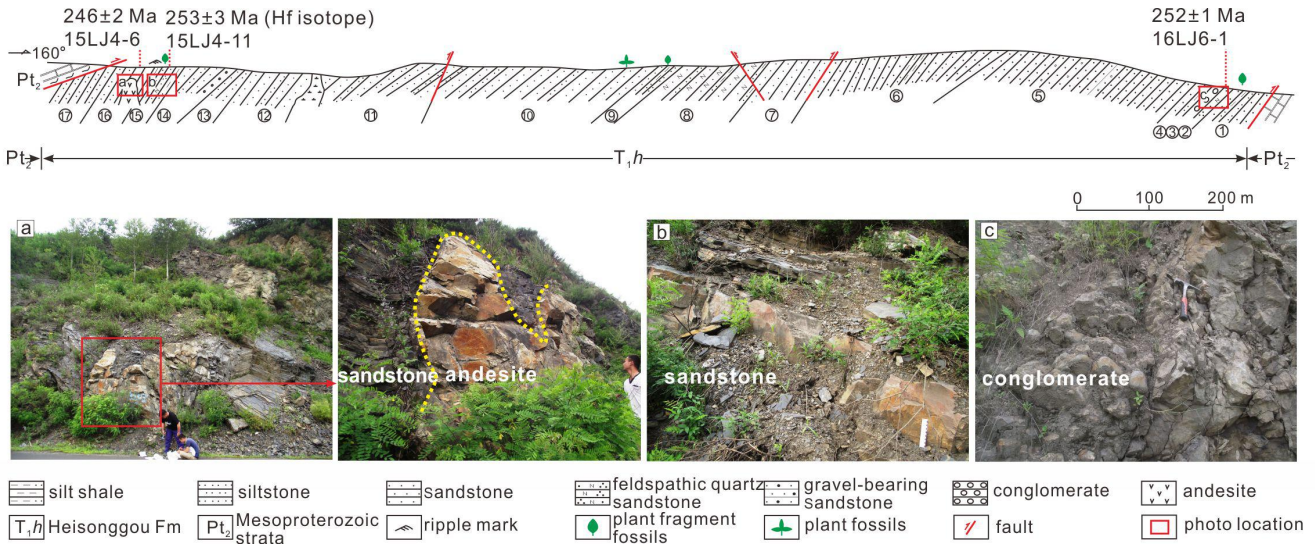
246±2 Ma
15LJ4-6
253±3 Ma (Hf isotope)
15LJ4-11
252±1 Ma
16LJ6-1
160°
Pt2
T1h
0 100 200 m
a
b
c
sandstone andesite
sandstone
conglomerate
silt shale
siltstone
sandstone
feldspathic quartz sandstone
gravel-bearing sandstone
conglomerate
andesite
T1h Heisonggou Fm
Pt2 Mesoproterozoic strata
ripple mark
plant fragment fossils
plant fossils
fault
photo location

Figure 5


72°
54(m)
45
36
27
18
9
0
(Hf isotope) 224±3 Ma 113±2 Ma
15JFS1-1 15JFS2-1
T_3x
a
conglomerate
stem fossil
b
diabase porphyrite
sandstone
diabase porphyrite
c
coal mine
0 100 m
223±2 Ma
16LJ8-1
113±3 Ma
15JFS10-1
K_1g
d
allgovite
e
tuffaceous siltstone
f
allgovite
g
pyroxene andesite
sandstone
pyroxene andesite
shale
silt shale
siltstone
tuffaceous siltstone
fine sandstone
feldspathic quartz sandstone
glutenite
conglomerate
coal
diabase porphyrite
pyroxene andesite
plant fossil
photo location
T_3x Xiaoyingzi Fm
K_1g Guosong Fm

Figure 6

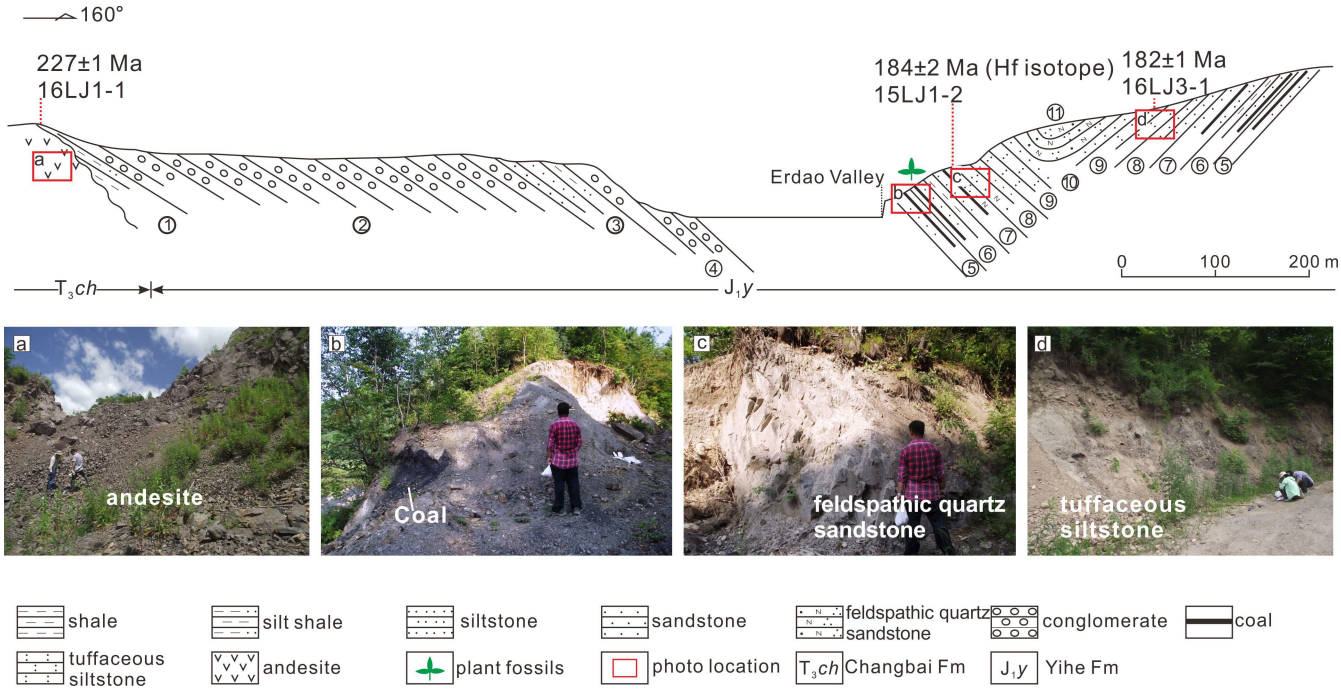
160°
227±1 Ma
16LJ1-1
184±2 Ma (Hf isotope)
15LJ1-2
182±1 Ma
16LJ3-1
Erdao Valley
a
b
c
d
① ② ③ ④ ⑤ ⑥ ⑦ ⑧ ⑨ ⑩ ⑪
0 100 200 m
T3ch
J1y
andesite
Coal
feldspathic quartz sandstone
tuffaceous siltstone
shale
silt shale
siltstone
sandstone
feldspathic quartz sandstone
conglomerate
coal
tuffaceous siltstone
andesite
plant fossils
photo location
T3ch Changbai Fm
J1y Yihe Fm

Figure 7

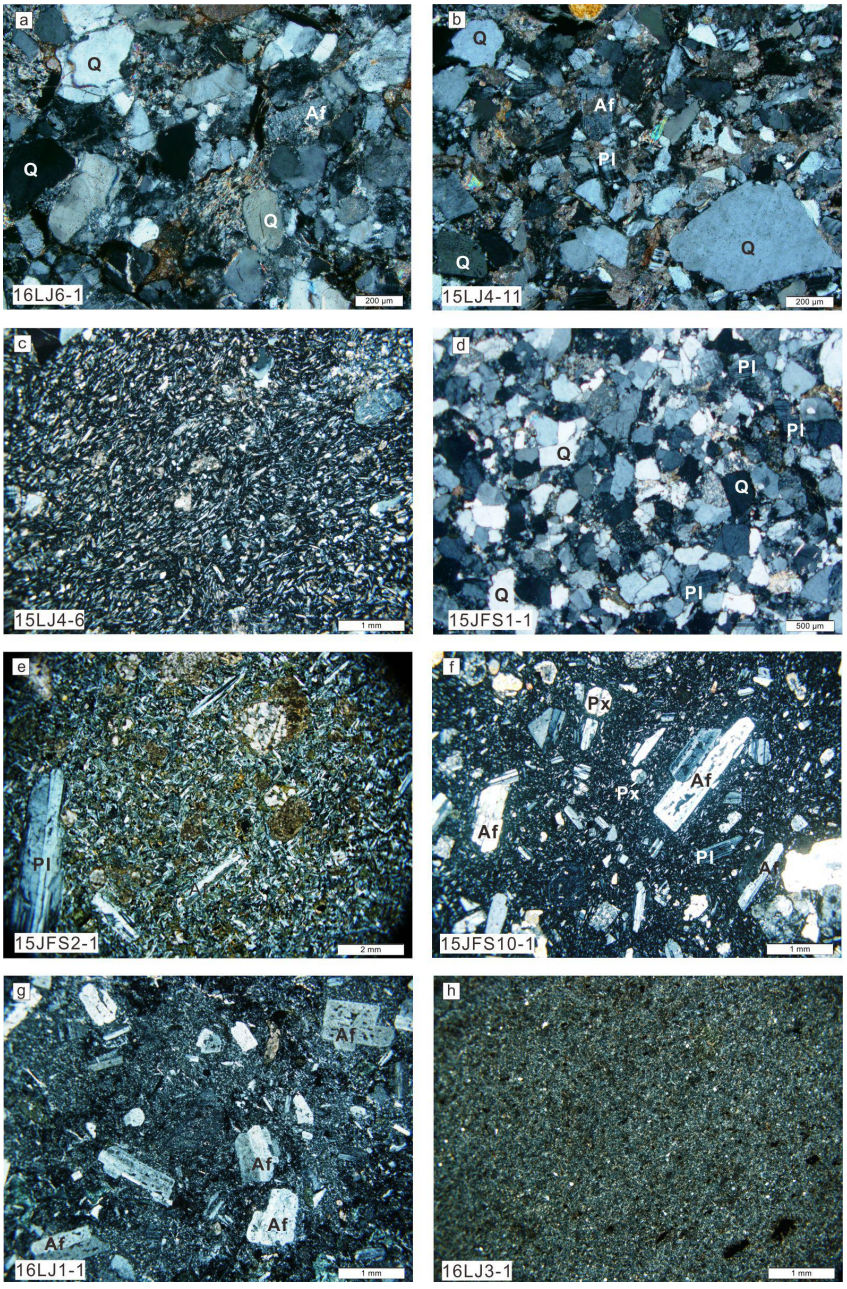
a
Q
Af
Q
Q
16LJ6-1
200 µm
b
Q
Af
Pl
Q
Q
15LJ4-11
200 µm
c
15LJ4-6
1 mm
d
Pl
Pl
Q
Q
Q
Pl
15JFS1-1
500 µm
e
Pl
15JFS2-1
2 mm
f
Px
Af
Px
Af
Pl
Af
15JFS10-1
1 mm
g
Af
Af
Af
Af
16LJ1-1
1 mm
h
16LJ3-1
1 mm

5

Figure 8

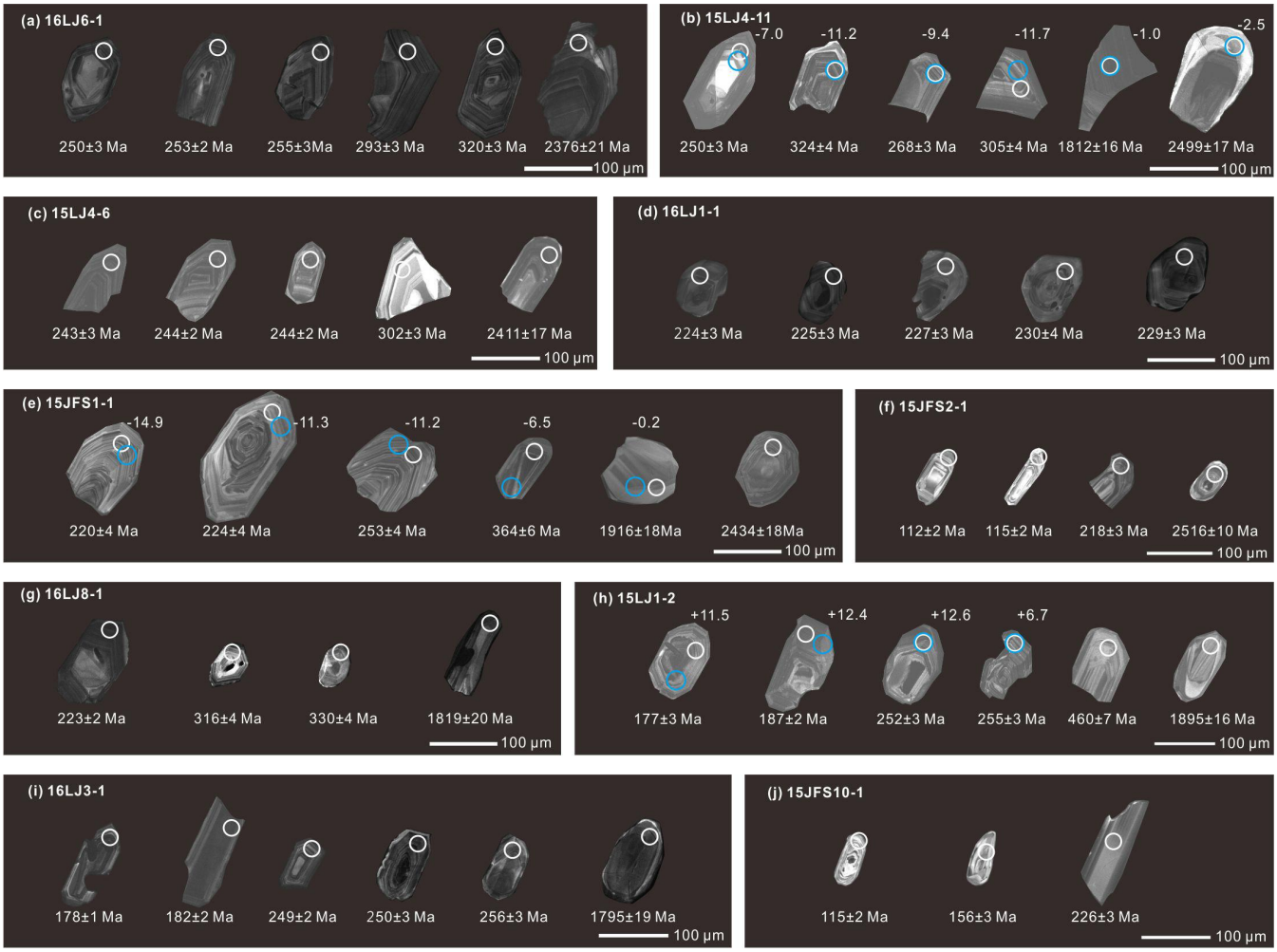
(a) 16LJ6-1
250±3 Ma
253±2 Ma
255±3Ma
293±3 Ma
320±3 Ma
2376±21 Ma
100 μm
(b) 15LJ4-11
-7.0
-11.2
-9.4
-11.7
-1.0
-2.5
250±3 Ma
324±4 Ma
268±3 Ma
305±4 Ma
1812±16 Ma
2499±17 Ma
100 μm
(c) 15LJ4-6
243±3 Ma
244±2 Ma
244±2 Ma
302±3 Ma
2411±17 Ma
100 μm
(d) 16LJ1-1
224±3 Ma
225±3 Ma
227±3 Ma
230±4 Ma
229±3 Ma
100 μm
(e) 15JFS1-1
-14.9
-11.3
-11.2
-6.5
-0.2
220±4 Ma
224±4 Ma
253±4 Ma
364±6 Ma
1916±18Ma
2434±18Ma
100 μm
(f) 15JFS2-1
112±2 Ma
115±2 Ma
218±3 Ma
2516±10 Ma
100 μm
(g) 16LJ8-1
223±2 Ma
316±4 Ma
330±4 Ma
1819±20 Ma
100 μm
(h) 15LJ1-2
+11.5
+12.4
+12.6
+6.7
177±3 Ma
187±2 Ma
252±3 Ma
255±3 Ma
460±7 Ma
1895±16 Ma
100 μm
(i) 16LJ3-1
178±1 Ma
182±2 Ma
249±2 Ma
250±3 Ma
256±3 Ma
1795±19 Ma
100 μm
(j) 15JFS10-1
115±2 Ma
156±3 Ma
226±3 Ma
100 μm

Figure 9

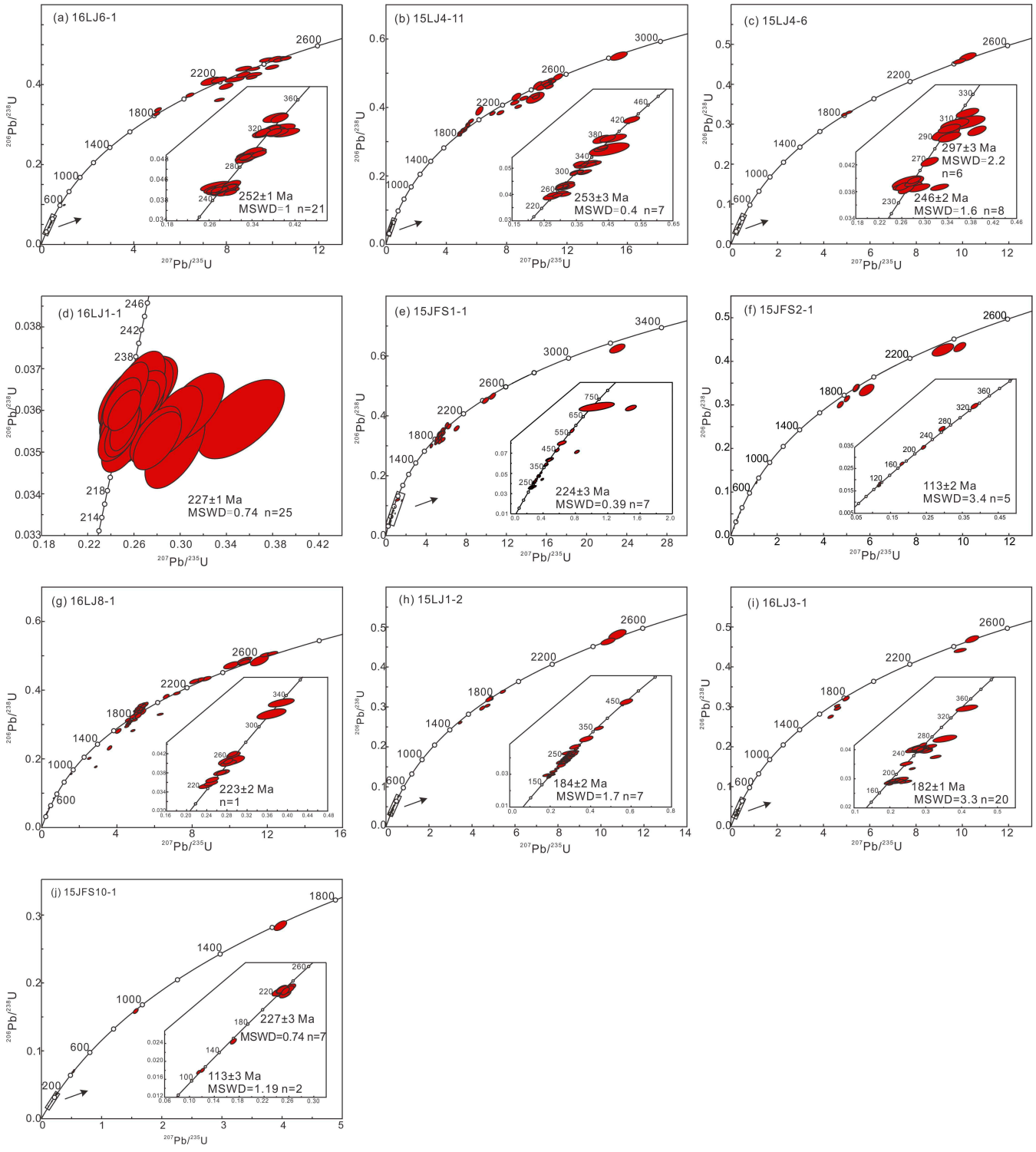
(a) 16LJ6-1
252±1 Ma
MSWD=1 n=21
(b) 15LJ4-11
253±3 Ma
MSWD=0.4 n=7
(c) 15LJ4-6
297±3 Ma
MSWD=2.2
n=6
246±2 Ma
MSWD=1.6 n=8
(d) 16LJ1-1
227±1 Ma
MSWD=0.74 n=25
(e) 15JFS1-1
224±3 Ma
MSWD=0.39 n=7
(f) 15JFS2-1
113±2 Ma
MSWD=3.4 n=5
(g) 16LJ8-1
223±2 Ma
n=1
(h) 15LJ1-2
184±2 Ma
MSWD=1.7 n=7
(i) 16LJ3-1
182±1 Ma
MSWD=3.3 n=20
(j) 15JFS10-1
227±3 Ma
MSWD=0.74 n=7
113±3 Ma
MSWD=1.19 n=2
$^{206}Pb/^{238}U$
$^{207}Pb/^{235}U$

Figure 10

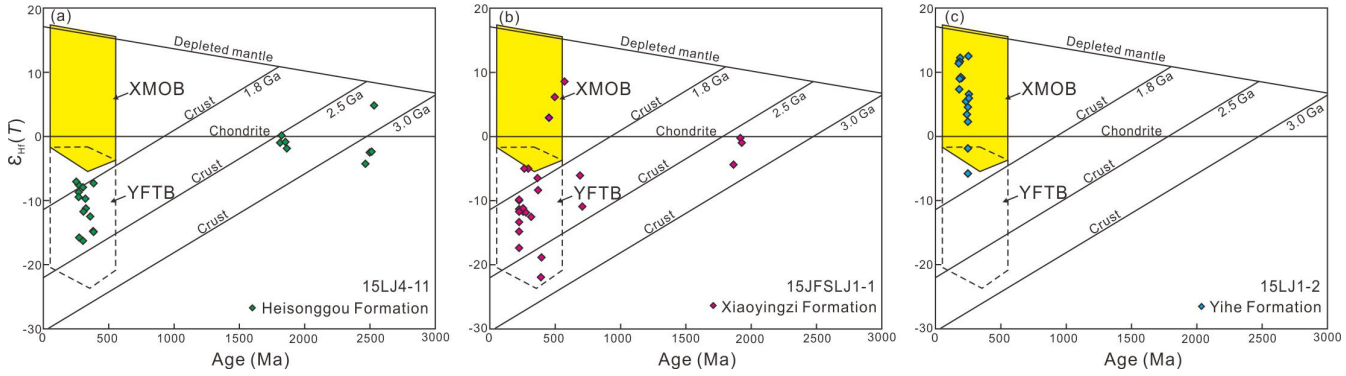
(a)
(b)
(c)
Depleted mantle
XMOB
YFTB
Crust
1.8 Ga
2.5 Ga
3.0 Ga
Chondrite
$\varepsilon_{Hf}(T)$
Age (Ma)
15LJ4-11
Heisonggou Formation
15JFSLJ1-1
Xiaoyingzi Formation
15LJ1-2
Yihe Formation

Figure 11

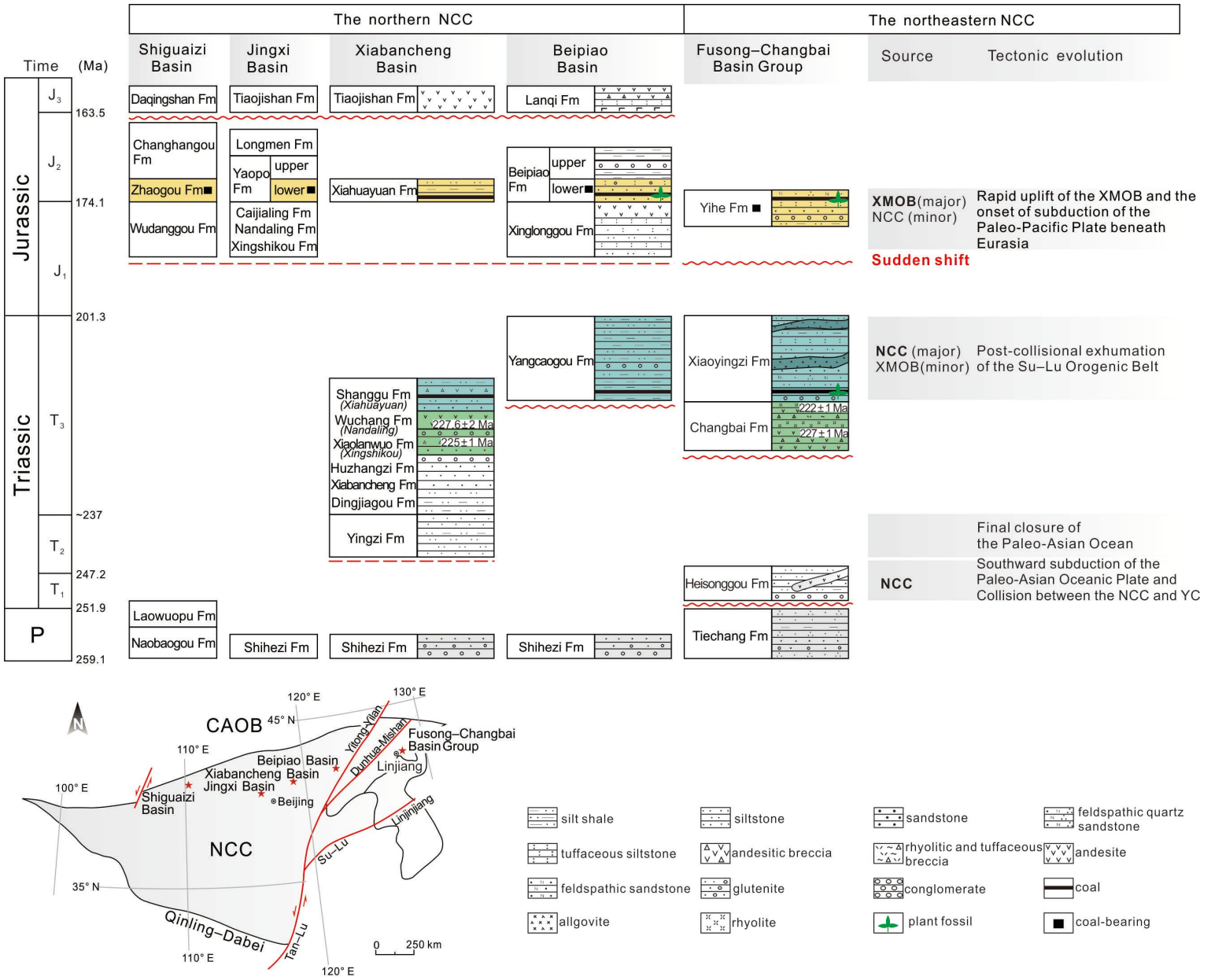
The northern NCC
The northeastern NCC
Time (Ma)
Shiguaizi Basin
Jingxi Basin
Xiabancheng Basin
Beipiao Basin
Fusong–Changbai Basin Group
Source
Tectonic evolution
Jurassic
Triassic
P
J3
J2
J1
T3
T2
T1
163.5
174.1
201.3
~237
247.2
251.9
259.1
Daqingshan Fm
Tiaojishan Fm
Tiaojishan Fm
Lanqi Fm
Changhangou Fm
Zhaogou Fm
Wudanggou Fm
Longmen Fm
Yaopo Fm
upper
lower
Caijialing Fm
Nandaling Fm
Xingshikou Fm
Xiahuayuan Fm
Beipiao Fm
upper
lower
Xinglonggou Fm
Yihe Fm
XMOB(major)
NCC(minor)
Rapid uplift of the XMOB and the onset of subduction of the Paleo-Pacific Plate beneath Eurasia
Sudden shift
Yangcaogou Fm
Xiaoyingzi Fm
Changbai Fm
222±1 Ma
227±1 Ma
NCC (major)
XMOB(minor)
Post-collisional exhumation of the Su–Lu Orogenic Belt
Shanggu Fm
(Xiahuayuan)
Wuchang Fm
(Nandaling)
Xiaolanwuo Fm
(Xingshikou)
227.6±2 Ma
225±1 Ma
Huzhangzi Fm
Xiabancheng Fm
Dingjiagou Fm
Yingzi Fm
Final closure of the Paleo-Asian Ocean
Heisonggou Fm
NCC
Southward subduction of the Paleo-Asian Oceanic Plate and Collision between the NCC and YC
Laowuopu Fm
Naobaogou Fm
Shihezi Fm
Shihezi Fm
Shihezi Fm
Tiechang Fm
CAOB
NCC
45° N
35° N
120° E
130° E
110° E
100° E
Yitong-Yilan
Dunhua-Mishan
Fusong–Changbai Basin Group
Linjiang
Beipiao Basin
Xiabancheng Basin
Jingxi Basin
Beijing
Shiguaizi Basin
Linjinjiang
Su-Lu
Qinling–Dabei
Tan-Lu
0 250 km
silt shale
siltstone
sandstone
feldspathic quartz sandstone
tuffaceous siltstone
andesitic breccia
rhyolitic and tuffaceous breccia
andesite
feldspathic sandstone
glutenite
conglomerate
coal
allgovite
rhyolite
plant fossil
coal-bearing

Figure 12

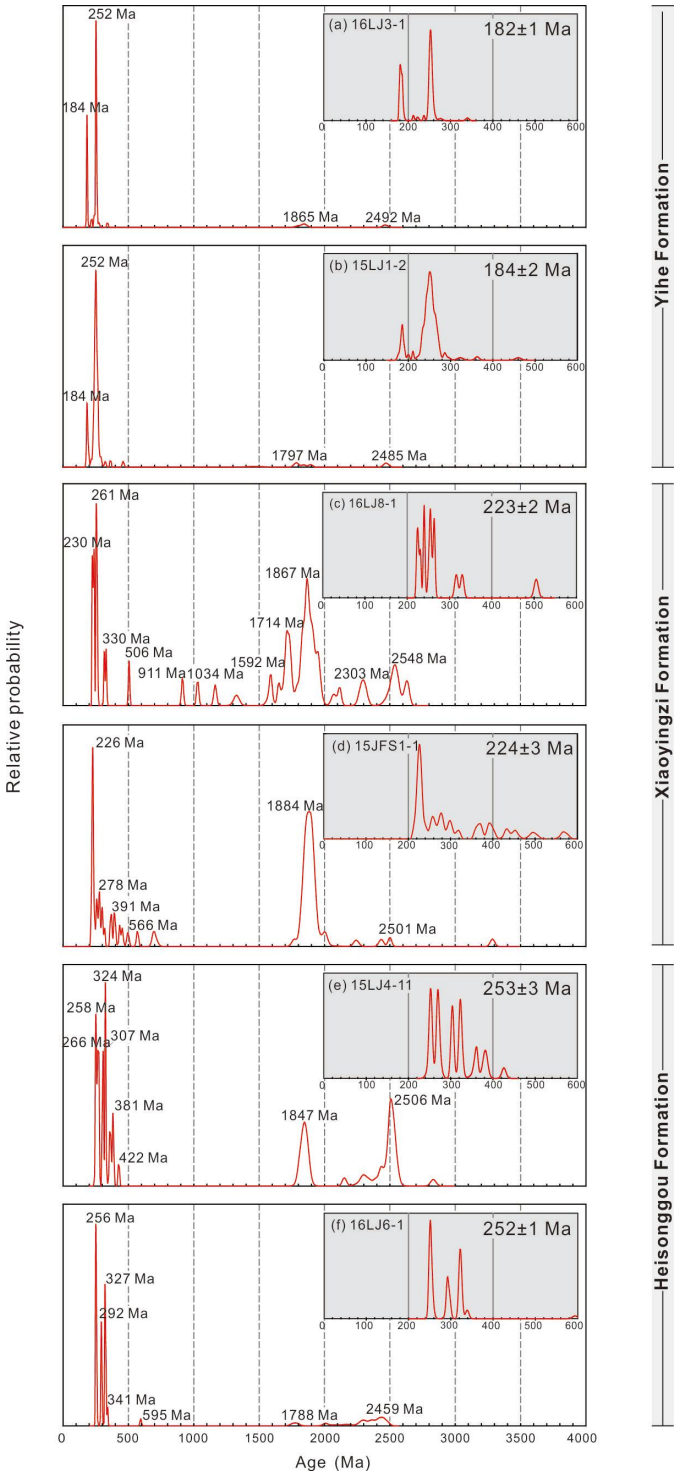
252 Ma
184 Ma
1865 Ma
2492 Ma
(a) 16LJ3-1
182±1 Ma
252 Ma
184 Ma
1797 Ma
2485 Ma
(b) 15LJ1-2
184±2 Ma
Yihe Formation
261 Ma
230 Ma
330 Ma
506 Ma
911 Ma
1034 Ma
1592 Ma
1714 Ma
1867 Ma
2303 Ma
2548 Ma
(c) 16LJ8-1
223±2 Ma
226 Ma
278 Ma
391 Ma
566 Ma
1884 Ma
2501 Ma
(d) 15JFS1-1
224±3 Ma
Xiaoyingzi Formation
324 Ma
258 Ma
266 Ma
307 Ma
381 Ma
422 Ma
1847 Ma
2506 Ma
(e) 15LJ4-11
253±3 Ma
256 Ma
327 Ma
292 Ma
341 Ma
595 Ma
1788 Ma
2459 Ma
(f) 16LJ6-1
252±1 Ma
Heisonggou Formation
Relative probability
0
500
1000
1500
2000
2500
3000
3500
4000
Age (Ma)

Figure 13

(a) Early Triassic: southward subduction of the Paleo-Asian oceanic plate, and subduction and collision between the NCC and YC

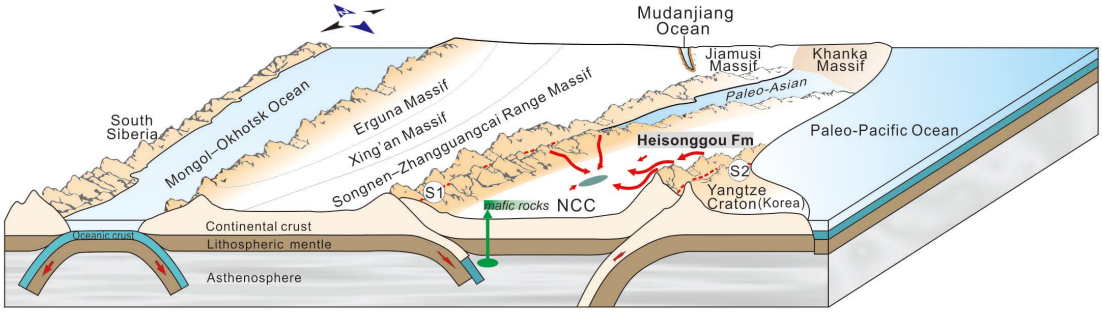

(b) Late Triassic: final closure of the Paleo-Asian Ocean and post-collisional exhumation of the Su-Lu Orogenic Belt

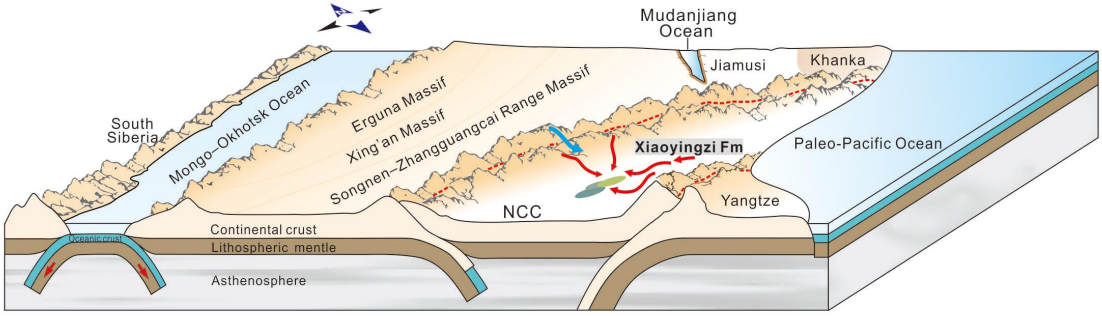

(c) Early Jurassic: rapid uplift of the XMOB and the onset of subduction of the Paleo-Pacific Plate beneath Eurasia